Master's thesis

NTNU
Norwegian University of Science and Technology

Timothée Dano

Experimental investigation of a high-temperature heat pump for food processing applications

Master's thesis in Sustainable energy
Supervisor: Armin Hafner
Co-supervisor: Shuai Ren
June 2023

NTNU
Norwegian University of
Science and Technology

Timothée Dano

Experimental investigation of a high-temperature heat pump for food processing applications

Master's thesis in Sustainable energy
Supervisor: Armin Hafner
Co-supervisor: Shuai Ren
June 2023

Norwegian University of Science and Technology

NTNU
Norwegian University of
Science and Technology

Table of Contents

List of Figures

List of Tables

Nomenclature

Acronyms

$ACHP$ Absorption compression heat pump

COP Coefficient of performance

$HACHP$ Hybrid absorption compression heat pump

HP Heat pump

$HTHP$ High temperature heat pump

IHX Internal heat exchanger

Greek Symbols

α Heat transfer coefficient ($\mathrm{W\,m^{-2}\,K^{-1}}$)

α_{lo} Liquid only heat transfer coefficient ($\mathrm{W\,m^{-2}\,K^{-1}}$)

α_{vo} Vapor only heat transfer coefficient ($\mathrm{W\,m^{-2}\,K^{-1}}$)

η Viscosity ($\mathrm{Pa\,s}$)

η_{is} Isentropic efficiency ($-$)

η_{Lorenz} Lorenz efficiency of the heat pump ($-$)

λ Thermal conductivity ($\mathrm{Wm^{-1}K^{-1}}$)

λ Volumetric efficiency ($-$)

μ Viscosity ($\mathrm{Pa\,s}$)

ϕ Enlargement factor ($-$)

ψ Built-in volume ratio of screw compressor

ρ_l Liquid density in the mixture ($\mathrm{kg\,m^{-3}}$)

ρ_v vapor density in the mixture ($\mathrm{kg\,m^{-3}}$)

φ Corrugation inclination angle ($\circ\,\mathrm{C}$)

ξ Moody friction factor ($-$)

ξ_0 Moody friction factor for straight longitudinal flow ($-$)

$\xi_{1.0}$ Moody friction factor for wavy longitudinal flow ($-$)

Roman Symbols

b Depth of the plate in the heat exchanger ($-$)

Bo Boiling number($-$)

cp Specific heat capacity ($\mathrm{K\,kg^{-1}\,K^{-1}}$)

d compressor displacement ($\mathrm{m^3}$)

Dh Hydraulic diameter (m)

F Chisholm´s two-phase enhancement factor ($-$)

G Mass flux ($\mathrm{kg\,s^{-1}m^{-2}}$)

h_{lv} Latent heat of evaporation ($\mathrm{J\,kg^{-1}}$)

K Proportional gain of controller in Dymola ($-$)

N compressor speed (Hz)

Nch Number of channels of the heat exchanger ($-$)

$Nplates$ Number of plates of the heat exchanger ($-$)

Nu Nusselt number ($-$)

p_{HP} Low pressure (Pa)

p_{int} Intermediate pressure of in the case of intercooling (Pa)

p_{LP} High pressure (Pa)

Pr Prandtl number (−)

q'' Heat flux ($\mathrm{W\,m^{-2}}$)

q Vapor quality (−)

R Circulation ratio (−)

Re Reynolds number (−)

$T_{log,mean}$ Logarithmic mean temperature ($\circ$ C)

Ti Time constant of the PI controller in Dymola (s)

u_{SL} Liquid velocity in the mixture ($\mathrm{m\,s^{-1}}$)

u_{SV} Vapor velocity in the mixture ($\mathrm{m\,s^{-1}}$)

V_1 Volume at the inlet of screw compressor ($\mathrm{m^3}$)

V_2 Volume at the outlet of screw compressor ($\mathrm{m^3}$)

V_{in} Working fluid volume flow at the entrance of the compressor ($\mathrm{m^3}$)

V_S Stroke volume ($\mathrm{m^3}$)

W Width of the heat exchanger plate (m)

W_{is} Isentropic work (W)

W_{shaft} Shaft work (W)

X_{tt} Lockhartt- Martinelli factor (−)

xr Ammonia-water ratio (−)

Z Correcting factor for absorption heat transfer (−)

1 Preface

This master thesis has been completed at the Norwegian University of Science and Technology during the spring semester of 2023. This work is part of a European program called ENOUGH which aims at reducing the greenhouse gas emissions in the food industry. It takes place as the concluding work of the Master program Sustainable Energy (*Heat pumping processes and systems*) in the department of Energy and Process Engineering.

My supervisor, Armin Hafner, deserves to be thanked for his advises and the feedbacks he has provided to complete this work.

I am also extending my thanks to Khalid Hamid who explained the functioning of the lab to me and was happy to answer my questions. In addition, I would like to give a special thanks to my co-supervisor Shuai Ren for all the help she has given and all the patience and reactivity she demonstrated. Last but not least, I would like to thank all my friends who supported me.

2 Abstract

Nowadays, most of the steam production for food processing purposes involves fossil fuels. To adress the climate change issue, it is urgent to promote the development of eco-friendly solutions for steam production. Absorption compression heat pump (ACHP) that utilizes ammonia-water as a working fluid is a promising option for high temperature industrial heat pumps due to the unique properties of zeotropic mixtures. These properties include non-isothermal phase change and lower vapor pressures. This report investigates the requirements of the food industry and the ways in which the ACHP can fulfill these needs. Potential solutions for heat exchangers and compressors are analyzed. The experimental setup of an ACHP at NTNU is presented and a simulation model of it on Dymola is established. Different cases are analyzed involving temperature lift up to 70 K and heating capacity of 100 kW. The cycle COP was up to 4.47 leading to potential greenhouse gas emission reductions up to 98.5 %. The influence of key parameters like the injection ratio or the sink and source inlet temperature were examined to determine the optimal operating conditions.

3 Summary

3.1 English

The food industrial sector requires a significant quantity of high temperature heat for its operations, which is often obtained from sources that require a large load of primary energy. However, there is a vast amount of low-grade surplus heat that goes to waste instead of being utilized. By using a heat pump to upgrade this heat to a higher temperature, primary energy can be saved. The hybrid heat pump, also known as the compression absorption heat pump, is an effective solution for this purpose.

In this report, a literature review is conducted to examine the specific demand for food processing systems. The focus of the review is on the operations of industrial high temperature heat pumps, with a particular emphasis on the features of ammonia as a working fluid. The review also examined the compressor and heat exchangers, two of the major components of the high temperature heat pump.

The report then describes an experimental facility built by NTNU to investigate the possibility of achieving sink outlet temperatures up to 160°C, using the Osenbrück cycle. The objectives and challenges of this demonstrator are highlighted, as well as the safety measures in place in the experimental area.

The report also presents a numerical simulation of the aforementioned cycle made on the software Dymola. The results of the simulation are discussed and a comparison is made with the experimental data.

Finally potential future work is suggested and a bibliography provides a summary of all the references cited in the report.

3.2 Norsk

Matindustrisektoren krever en betydelig mengde høy temperatur for sine operasjoner, som ofte er hentet fra kilder som krever en stor mengde av primær energi. Imidlertid er det en stor mengde lavtemperaturs overskuddsvarme som går til spille i stedet for å bli utnyttet. Ved å bruke en varmepumpe til å oppgradere denne varmen til en høyere temperatur kan primærenergi spares. Hybridvarmepumpen, også kjent som kompresjons-absorbsjonsvarmepumpen, er en effektiv løsning for dette formålet.

I denne rapporten er det gjennomført en litteraturgjennomgang for å undersøke den spesifikke etterspørselen etter matprosesseringssystemer. Fokuset for gjennomgangen er på driften av industriell høytemperatursvarmepumper, med spesiell vekt på funksjonene til ammoniakk som arbeidsvæske. Gjennomgangen undersøkte også kompressor og varmevekslere, to av hovedkomponentene i høytemperatursvarmepumpen.

Rapporten beskriver deretter et forsøksanlegg bygget av NTNU for å undersøke muligheten for å oppnå synkeutløpstemperaturer opp til 160°C ved bruk av Osenbrück-syklusen. Målene og utfordringene til denne demonstratoren er fremhevet, samt sikkerhetstiltakene som er på plass i forsøksområdet.

Rapporten presenterer også en numerisk simulering av den nevnte syklusen laget på programvaren Dymola. Resultatene av simuleringen diskuteres og det gjøres en sammenligning med de eksperimentelle dataene.

Til slutt foreslås potensielt fremtidig arbeid, og en bibliografi gir et sammendrag av alle referansene som er sitert i rapporten.

4 Introduction

4.1 Motivation

The food industry is one of the major source of the greenhouse gas emissions (GHG). Globally, between 21 and 37% of the total emissions can be attributed to the systems of this industry. Increasing energy efficiency and reducing the use of fossil fuels are main leverages to reach climate neutrality in the food supply chain. The available waste heat potential in the EU is estimated around 300 TWh/year (the total industrial energy demand was 2950 TWh in 2015 in comparison). One third of this heat is below 200 °C and is considered as low temperature waste heat. Many industrial processes requiring both cooling and heating have separate systems for these purposes. Integrating heat pumps is a way to provide both heat demands while utilizing waste heat. This increases significantly the overall energy efficiency. Heat pumps reduce the primary energy required (electricity) by recovering available waste heat. This is reflected in a parameter defined as Coefficient of performance (COP). For instance, meat and dairy processes use both low and high temperature thermal processes, such as smoking, drying, chilling, thawing or pasteurization. The energy consumption could be reduced by integrating different processes utilizing the heat recovered from the low-temperature refrigeration system.

High-temperature heat pumps (HTPSs) are a promising technology to achieve both heat recovery and high energy efficiency. The HTHPs can combine heating and coolings processes and are able to achieve performance comparable to fossil fuel boilers. An interesting feature of these system is that they can be run with natural refrigerants such as CO_2 or Ammonia which have a low global warming potential.[1]

The Ammonia-water absorption-compression heat pump (ACHP) uses a mixture of ammonia and water as a natural working fluid and combines the technologies of an absorption and vapor compression heat pump. The ACHP is based on the Osenbrück cycle with a single stage solution circuit. The ammonia-water mixture has a large boiling temperature range. This allow the system to extract and release heat at gliding temperatures and so the compression ratio can be lower than for

conventionnal heat pumps. The ACHP can achieve high heat sink temperatures up to 140 °C which is comparable to fossil fuel boilers performances.

As the thermal demands in meat processes are specific, the applicability of the ACHP needs to be investigated and its performance must be optimized. The ACHP test rig in NTNU can provide an experimental system for an investigation and optimization of the operating parameters, conditions and components for the applications in meat processing.

4.2 The project ENOUGH

Figure 1: Enough project logo

The ENOUGH project is a European program which aims to reduce the greenhouse gas emissions of the food industry. To accomplish this, the project will develop tools and strategies to support the EU's Farm to Fork initiative in creating climate neutral food businesses. The project has the following objectives :

- *Identify* how to achieve climate neutrality for food businesses.
- *Improve* integrated sustainability and meet societal goals.
- *Increase* awareness among policy makers, businesses, investors, entrepreneurs, institutions, stakeholders and citizens of selected innovative systemic solutions and their potential for uptake at EU scale.

4.3 Literature review

Please note that since this is a continuation of the project assignment, a part of this section as well as section 5 is similar to the work previoulsy done in [2].

4.3.1 Food processing systems

Alia et al. (2019) present an overview of the energy requirements in the food industry [3]. Food plants produce a variety of products requiring freezing, chilling, grilling or steaming which create a demand of heat at several temperature levels. For example, rapid freezing at temperature below -40°C is required to preserve a good quality of the food product while process such as grilling or steaming represent a heat demand above 100 °C.

Alia et al. describe the dairy industry as one of the most energy intensive in the food sector. The dairy industry has low temperature requirements for refrigeration of the products but also high temperature needs for cleaning, evaporation and pasteurization. Pasteurization is a food process in which products such as milk or fruit juice are treated with mild heat (usually less than 100 °C) to eliminate pathogens and extend shelf life. Drying is also necessary in process involving milk powder.

The meat and fish production also represents one of the most energy demanding sector in the food industry. In order to provide convenient products for the consumers, the meat and fish product are often frozen. Freezing a product obviously represents more energy demand than cooling. For example, freezing of pastries represents more than one third of the total energy demand in the process.

Most of food companies usually have facilities for the production of refrigeration and steam which run independently. The ACHP has the capability of delivering hot water up to more than 100 °C by recovering waste heat at approximately 50 °C. This heat pump is thus able to recover heat from the refrigeration facility in order to produce hot water as emphasized by Nordvedt (2013) [4].

Nordvedt worked on the example of a slaugtherhouse in RUDSHØGDA which required large amounts of hot process water at minimum temperature of 83 °C. An

ACHP of 650 kW has been installed there working with a reciprocating ammonia compressor and plate heat exchangers. The desorber is exchanging heat with waste heat from the cooling/freezing plant at a temperature around 50 °C. The hybrid heat pump delivers water at a temperature of 87 °C which is delivered to a secondary circuit. This avoid contamination of water by ammonia in case of leakage. A second low-presure ammonia heat pump was used to pre-heat the process water. This installation was coupled with a hot water accumulator tank in order to give flexibility to the production. Thanks to this tank, the system can manage large hot water demand without huge peaks of the heating system. According to Nordvedt, this ACHP working with an average efficiency of 4,5 over three years is helping save 3.4 GWh annually. Ahrens et al. [5] presents another example of how the ACHP can be used in an actual food processing plant. The temperature levels are as following : around 115 °C for cooking, 90 °C for cleaning and 50 °C for the building heat correspond to the heating demand. Concerning the cooling demand, the plant under scrutiny requires air conditioning at a temperature between 5°C and 20°C, chilling at -5°C and freezing at -40°C. Multiple scenario for the system arrangement are analysed in this study but the most interesting one is involving a ACHP which satisfy the heating demand at the temperature level between 80 °C and 95°C.

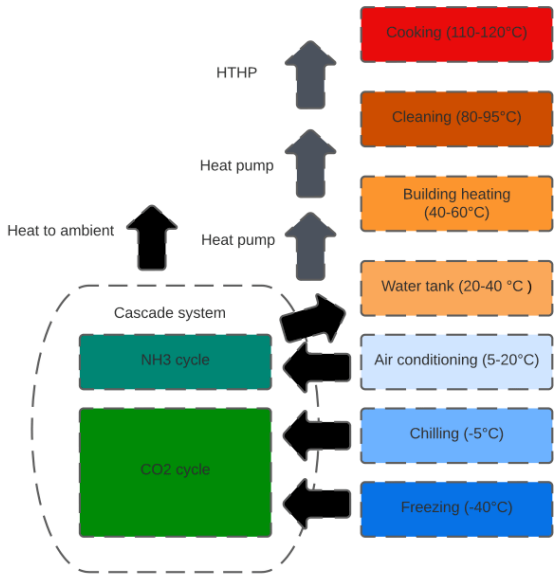

Figure 2: Simplified representation of the fully integrated system

In this arrangement, a CO_2/NH_3 cascade refrigeration system is used to satisfy

the freezing demand, the cooling demand and the air conditioning. The condensing heat is rejected to a 20/40 °C water tank which is connected to the building heating system through a NH_3 heat pump. The ACHP uses the integrated water tank of the building heating system as a heat source. This allows production of hot water up to 95°C with moderate pressure ratio that can be used for cleaning purposes. Finally, a high-temperature heat pump uses the water tank of the cleaning process as a heat source to deliver heat at a temperature up to 120 °C for the cooking process. In this fully integrated configuration, all heat demands are satisfied thanks to internal heat recovery through heat pumps. This scenario is represented in Figure 2.
According to Ahrens et al., this fully integrated configuration reduce the total power consumption (electrical) by almost 40 % compared to a scenario in which the different thermal demands are satisfied separately by different systems or equipments. Concerning GHG emissions, this configuration allow a reduction of up to 45 % if we consider a site in Norway previously using electricity and gas boilers. To conclude, considering growing amounts of renewable energy sources in the electricity mix of most countries, the integration of heat pumps or HTHP coupled with heat storage tank can lead to tremendous reduction of greenhouse gas emissions in the food industry. Similar investigation have been conducted more recently by Ahrens et al (2021) on a dairy plant achieving GHG emission reduction up to 92% [6].

4.3.2 State-of-the-art

Ahrens et al. (2018) [7] explain that ammonia-water hybrid heat pumps combining absorption and compression processes have proven their reliability and functionality in the industrial sector using standard components. The paper shows that the compressor is the most critical component to achieve high pressure and temperature levels. According to a study from the same author focusing on the compressor (2019) [8], available compressors on the market cannot operate with such high pressure or achieve exit temperatures higher than 140 °C. In order to improve the system, adjustments have to be made like the division of the compression process or the integration of additional cooling options. Concerning the heat exchangers, Nordtvedt (2005) [9], described different possibilities. Plate heat exchangers are a promising

possiblities as they have a compact design and good mixing conditions. They exist in two different absorption modes : falling film mode or bubble mode which have both advantages and challenges. The characteristics of these two modes will be detailed further in section 5. Nevertheless, as emphasized by [7], design and efficiency of the absorber and desorber might not be optimal due to the lack of knowledge and experience on the subject. The compressor solutions exist on the market but they need to be discussed and improved to run in the specific operating conditions. That is why, a ACHP test facility containing the entire cycle has been built in NTNU in order to gain experience on the operating conditions and improve the main components. This facility can serve as a starting point for further research by combining possible solutions and experimental results and demonstrate potential approaches to improve the application range and efficiency.

4.4 Objectives

In his doctoral thesis published recently [10] , Marcel Ahrens explains the solutions and challenges for the achievement of a ACHP running at high temperature. Important features of this system are the compressor design with respect to discharge temperature and lubrication, the design and operation of the heat exchangers and the selection of the solution pump. Thus, the following objectives are proposed :

- Explain the functioning of the system and detail the reason for each component choice based on the aforementioned thesis.
- Perform initial experiments with the HTHP cycle.
- Simulate numerically the cycle as precisely as possible in order to be able to predict the behavior of the lab cycle.
- Determine the operating parameters that allow a steady state both numerically and experimentally. In theory, ACHP have the ability to achieve supply temperature up to 120 °C with temperature lift up to 60 K and temperature glide up to 30 K.

- Investigate parameters such as the circulation ratio and the sink and source temperatures in order to find the optimal conditions to reach high efficiency and the characteristics mentioned above.
- Analyse the results (simulation versus experimental) in terms of system performance, power demand and GHG emissions (depending on the energy/power mix across the globe).

4.5 Report outline

This report is structured by seven parts containing an overview and a summary of the work conducted for the master thesis. These chapters can be outlined as :

- **Part 4** Introduces the motivation for the work and highlights the objectives of the report
- **Part 5** Provides the background concerning absorption-compression heat pump with water-ammonia as refrigerant. The properties of ammonia are investigated and the Osenbrück cycle is described. The choices of the main components of the cycle are also justified.
- **Part 6** Addresses the methodology of the numerical investigation conducted on the sofware Dymola and presents the NTNU ACHP facility.
- **Part 7** Presents the results obtained with the simulation and in the lab.
- **Part 8** Offers a discussion on the results regarding the differences between experimention and numerical investigation, source of errors and comparison to results found in the literature.
- **Part 9** Concludes the report by presenting the main findings and the contribution of it to to ACHP technology at high temperature.
- **Part 10** Suggests possibilities for further work that could follow in order to additionally improve the investigated system both experimentally and theoretically.

5 Background

This section provides the necessary background to make the content of this report understandable to the reader. It presents the characteristics of ammonia as a working fluid and the main features of an absorption-compression heat pump. It also details the choice of components such as the compressor, the heat exchangers and the solution pump for the experimental ACHP based on a state-of-the-art analysis.

5.1 Ammonia as a working fluid

During the 19th century, the refrigeration industry was using gases such as ammonia (NH_3), methyl chloride (CH_3CI) or sulphur dioxide (SO_2) but this lead to numerous accidents because of the toxicity of these substances [11]. This is why a new search began for solutions that were not dangerous for humans. In the 20th century, the CFCs (Chlorofluorocarbon refrigerant gases) were developed for household refrigerators because they were non toxic-toxic and non flammable. Nevertheless, it was later discovered that the CFCs are damaging the ozone layer that shields the earth from UV light. In order to solve that problem, the HFCs (halogenated hydrocarbons) were discovered as a substitute. However, these substances having a high global warming potential, it became clear that they had no commercial future after Paris Climate agreement (2015) and Montreal Protocol Amendment of Kigali (2016). In order to ensure sustainability, it seems a reasonable solution to use natural refrigerants that have been integrated in nature for millions of years. There were considerable researchs on natural refrigerants like CO_2 or Ammonia in the last two decades which led to the first installations on the market around 2000.

5.1.1 Characteristics of Ammonia

Main features

The thermodynamic properties of ammonia (also called R717 in the refrigeration industry) are very favorable towards using it as a working fluid. Its specific heat

capacity is very high and allows a particularly high heat transfer coefficient during evaporation of liquid and condensation. In addition, ammonia is much cheaper than any other fluorocarbon which makes it attractive for industrial purposes. Concerning toxicity, ammonia has a pungent smell which can be detected by humans at a concentration around 5 ppm but it represents a danger for life only above 5000 ppm. Therefore, the risk of inhaling dangerous amounts of Ammonia is quite reduced. Ammonia is considered to have a neutral global warming potential as it can dissolve in water and atmosphere and then act as a nitrogen-rich fertilizer for the plants. Moreover, NH_3 has a high volumetric cooling capacity (3100 kJ/m^3compared to 2080 kJ/m^3 for R134a for example). The critical temperature of ammonia is significantly higher than the one of all the other refrigerants which leads to a better energy efficiency for applications with high condensing temperature as highlighted by Eckert M. [11]

Critical temperature and pressure

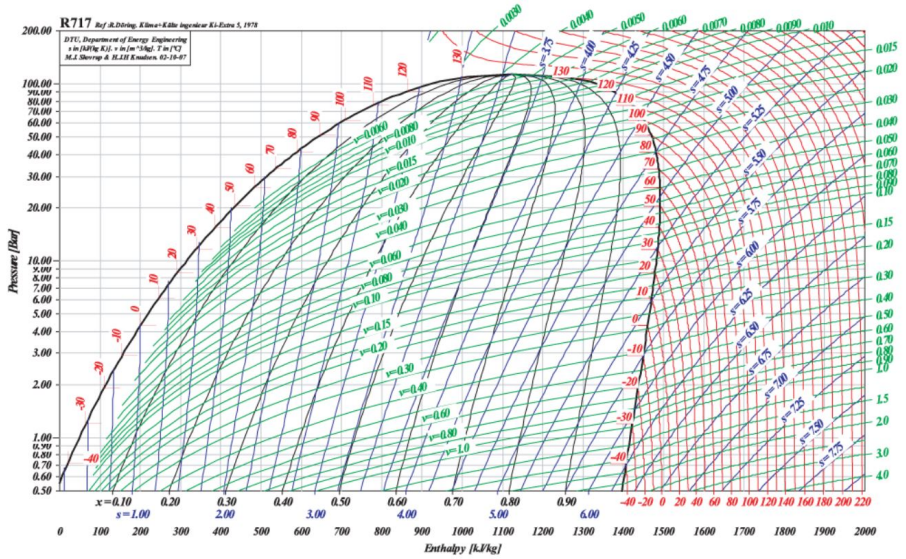

Figure 3: Log (P) - H diagram of R717 (NH_3), *COOLPACK*

Figure 3 shows the log (P) - H diagram of NH_3. The critical temperature of ammonia is 132.2 °C, this is higher than most of the refrigerant for which it is in the range 70-100 °C. If the condensing temperature gets closer to the critical temperature, the energy efficiency and the capacity of the system are dropping considerably. As ammonia has a high critical temperature, it is more suitable than most refri-

gerants for high-temperature heat pump applications. Besides, the critical pressure of ammonia is 113 bar contrary to the synthetic refrigerants which have a critical pressure of around 35-50 bar. Thus, the volumetric cooling capacity of ammonia is higher for high-temperature than synthetic refrigerants. This feature also allows ammonia to cover refrigeration applications with large temperature differences as those with high ambient temperatures.

Compressor discharge temperature

NH_3 has a high cp/cv ratio and this leads to very high compression end temperature. The properties of the lubrication oil can be impacted by these temperatures and this must be taken into account. The oil needs to stay stable at those temperatures and keep its lubricating properties.

Normal boiling point

The normal boiling point (NBP) of ammonia is -33,3 °C which means that NH_3 evaporates at this temperature and atmospheric pressure. This constraint is not as relevant for ammonia as for other refrigerants because NH_3 is still reliable if small amounts of water or air are drawn into the system.

Heat transfer

As ammonia have a high heat transfer coefficient, the surface area required to transfer a certain amount of heat is smaller than for HFCs. This leads to a smaller cost in machinery and piping. However, ammonia is incompatible with copper and might requires more expensive materials which offsets partially this advantage.

5.1.2 Zeotropic mixture

When mixed together, ammonia and water form a zeotropic mixture which will have a temperature glide during the phase change. As explained by Ahrens et al. (2019) [8], due to the lower boiling point of ammonia, when the temperature of the mixture increases, the concentration of ammonia in the liquid phase will decrease because

NH_3 evaporates. This will make the saturation temperature of the solution increase. This property can be adapted to gliding temperatures of both heat sinks and heat sources. The irreversibility of the system is lower because the temperature gap is smaller and thus the efficiency is better as [7] showed.

5.2 Absorption Compression Heat Pump

General principle

The principle of an hybrid absorption compression heat pump is to add a solution circuit to a conventional vapour compression heat pump. A simplified representation of the ACHP cycle is shown on Figure 4. An internal solution circuit is implemented parallel to the compressor from points (4) to (7). While flowing through the desorber, the ammonia-water mixture is in the two-phase region and the concentration of ammonia in the liquid phase is decreasing as NH_3 evaporates. The evaporation is incomplete so at point (1), it is a two-phase mixture that leaves the desorber. A liquid-vapour separator is used to set apart the phases so that only vapour continues toward the compressor (2). The liquid phase which has now a low concentration of ammonia (called "weak solution") flows through the solution pump (4) and its pressure increases (5). At this point, the weak solution goes through an internal heat exchanger (IHX) to increase the temperature (5-6). This exchanger helps to improve the overall cycle efficiency. The vapour flows through the compressor and its pressure is increased as well (3) before being mixed with the weak solution (7). At this point, the liquid-vapour mixture is ready to enter the absorber. In the absorber, as heat is provided to the heat sink, ammonia is absorbed into the liquid phase and thus the concentration of NH_3 increases. Between point (7) and (8), the weak solution turns into strong solution again. Then, this strong solution exchanges heat with the weak solution from the other side through the IHX before being expanded to the low-pressure level (9-10). Finally, the strong solution returns to the desorber so the cycle is looped.

As stated by Nordtvedt et al. [4], the evaporation and condensation processes will take place at gliding temperatures. The saturation temperature of NH_3 is considerably lower than the saturation temperature of water so when the concentration of ammonia increase in the absorber, the solution will cool down. On the contrary, in the desorber, as ammonia is evaporated, the saturation temperature of the solution will increase between the inlet and the outlet.

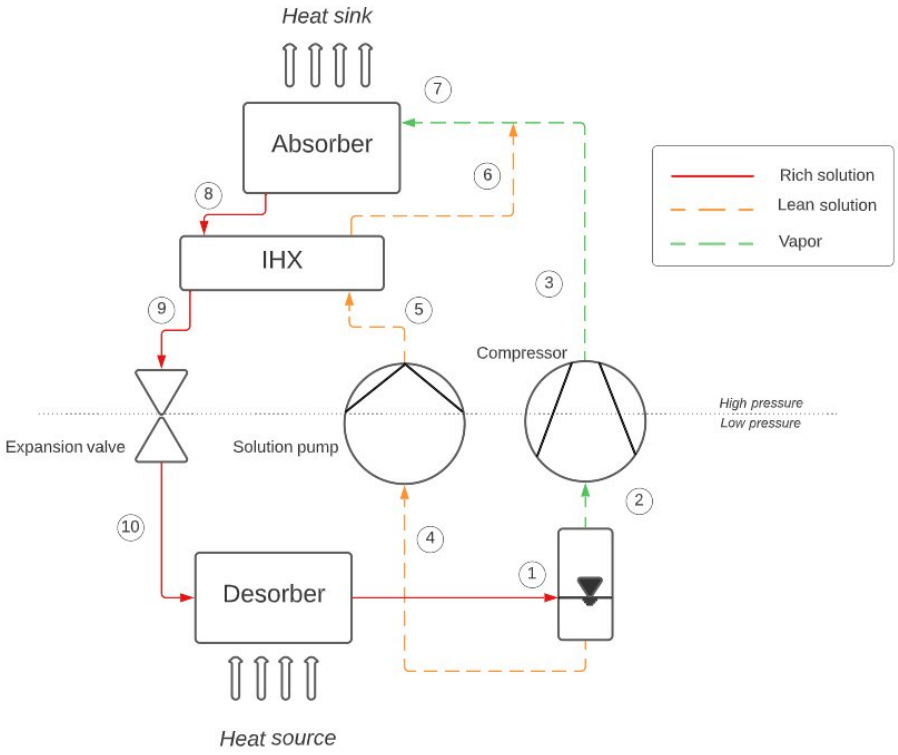

Figure 4: Simplified sketch of an absorption compression heat pump cycle

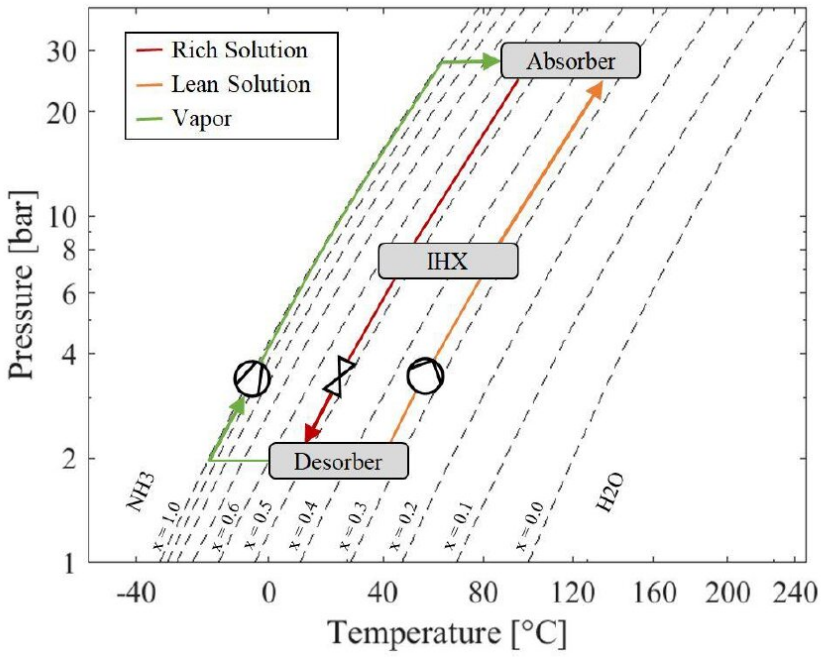

Figure 5: Pressure/Temperature diagram of saturated liquid for an ammonia-water mixture with hybrid heat pump components

High flexibility of ACHP

Jensen et al.[12] worked on the degrees of freedom of the ACHP allowed by the internal solution circuit. For a conventional vapour compression heat pump, the degrees of freedom are as following : the temperature glide (temperature difference between the inlet and the outlet of the sink and source), the temperature lift (difference between the sink outlet temperature and the source inlet temperature), the temperature out of the sink and the two mass flows of the sink and the source. For the ACHP, Jensen pinpoints that the circulation ratio CR and the rich ammonia mass fraction xr are also to be determined. The circulation ratio is defined as the ratio between the mass flow rate of the lean solution and the rich solution :

$$CR = \frac{\dot{m}_{lean}}{\dot{m}_{rich}} \tag{1}$$

xr is defined as the ratio between ammonia and water in the rich solution :

$$xr = \frac{m_{ammonia}}{m_{water}} \tag{2}$$

For a specified mass fraction of the rich solution, the ammonia mass fraction of the lean solution can be controlled through the circulation ratio. This modification of this circulation ratio is a way to change the temperature difference throughout the desorber and the absorber. Jensen showed that as soon as the ammonia mass fraction is above a certain value, it exists a circulation ratio that maximize the COP. This optimal circulation ratio will decrease if the ammonia mass fraction increases. According to Jensen (2016) [13] the best possible implementation in terms of overall efficiency is found with an ammonia mass fraction of 0.82 and circulation ratio of 0.43. For these reasons, it is important to determine the correct combination of mass fraction and circulation ratio in order to choose the design of the cycle. As the heat transfers in the absorber and desorber are non-isothermal, the definition of the COP is quite different than usual. For a cycle operating between constant heat source and sink temperature levels :

$$COP_{Carnot} = \frac{T_{sink}}{T_{sink} - T_{source}} \tag{3}$$

In our case, the theoretical limit value for the coefficient of performance will be determined as described by Lorenz (1895) :

$$COP_{Lorenz} = \frac{T_{log,mean,sink}}{T_{log,mean,sink} - T_{log,mean,source}} \tag{4}$$

The constant temperature levels are replaced by the logarithmic mean temperature of the heat sink and source :

$$T_{log,mean} = \frac{T_{in} - T_{out}}{\ln(\frac{T_{in}}{T_{out}})} \tag{5}$$

for a given secondary fluid.

As presented by Jensen et al. (2018) [14], a Lorenz efficiency can be derived as a ratio between the actual COP of the heat pump and the Lorenz COP as in Equation (6).

$$\eta_{Lorenz} = \frac{COP}{COP_{Lorenz}} \tag{6}$$

Changing the overall NH_3 mass fraction results in a change in the low-pressure gas density. All other parameters being unchanged in the compressor, the mass flow of the vapor evolves which leads to a different capacity. The advantage of an ammonia-water heat pump compared to a simple ammonia heat pump is that higher heat sink temperatures can be reached with lower discharge vapor pressure and reduced pressure ratio.

This ability to define more parameters than on a regular vapour compression heat pump makes it easier to adapt to variable heat capacities and temperature levels. As mentionned by Honghzi et al (2021) [15], the large temperature lift achievable with this ACHP can allow steam generation process which can be a sustainable heating system for industry.

5.3 Choice of main components

5.3.1 Identification of the main challenges

Ahrens conducted an investigation of all the previous experimental studies made on ACHP [10] and provided an overview of the identified challenges and their allocation in the system :

- **Heat exchangers** : Achieve an efficient and cost-effective absorber and desorber design. Understanding the occurring heat transfer phenomena is indispensable, especially for the absorber which is operating at high temperature and pressure.
- **Mixing** : Reach an efficient liquid vapor mixing and distribution process. Select appropriately the operation mode of the heat exchanger is the key to achieve high overall heat transfer coefficient.
- **Compressor** : Reduce the compressor discharge temperature and select a suitable lubrication system. Realize an oil-free system operation if possible. As additional components are required to handle oil-lubrication, this raise the complexity and costs of the system. Besides, the oil tends to penetrate the circuits and this requires a recirculation which lowers the heat pump performance. Nevertheless, oil-free operation also represents a challenge because it needs modification of the system and might not be available on the market. Thus, it is associated with higher equipment cost.
- **Solution pump** : As saturated liquid is leaving the liquid-vapor separator, a sudden modification in the low-pressure conditions can lead to vapor being drawn into the solution pump. This phenomena is called cavitation and has to be avoided not to damage the pump.

5.3.2 Cycle configuration

The most simple configuration of the ACHP cycle is the one shown on Figure 4. Various other configuration exist with different arrangements or with new components like desuperheater or cooling circuits.

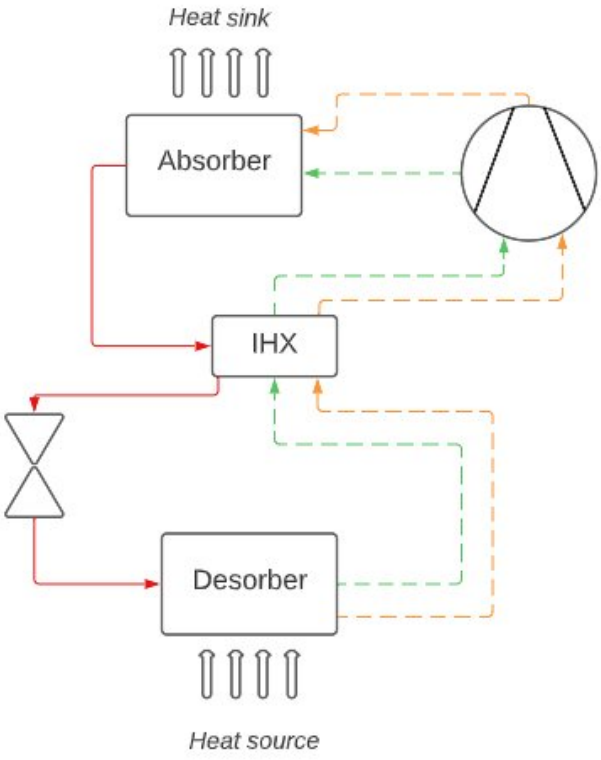

Figure 6: Schematic representation of a wet compression cycle

One of this cycle configuration is called the wet compression cycle, also known as wet compression-resorption cycle and is shown on Figure 6. This configuration was investigated in particular by Itard and Machielsen (1994) [16]. Whereas dry compression cycle has a separate solution circuit, the wet compression cycle convey the ammonia-water mixture as a wet-vapor state through the compressor. Therefore, the compression takes place in the two-phase state which reduces the compressor discharge temperature and the required compression work because the superheating of the vapor is reduced. This system needs a good internal heat exchange and a compressor with high isentropic efficiency in order to achieve high performance. The flexibility of this configuration is reduced as the circulation ratio and the mixture composition are both fixed.

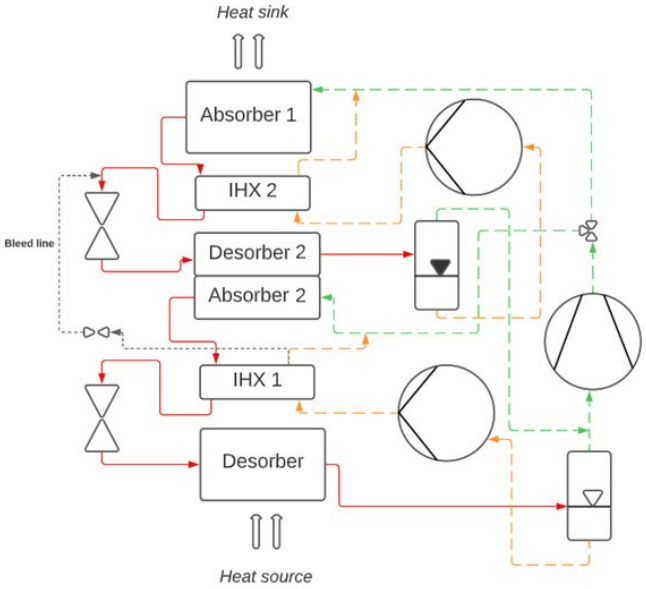

Figure 7: Schematic representation of an ACHP with two-stage solution circuit

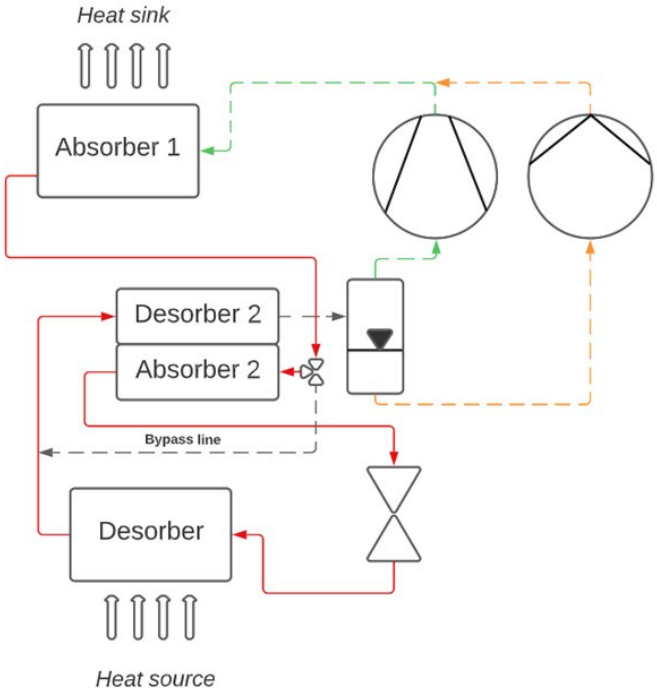

Figure 8: Schematic representation of a ACHP with single circuit and desorber/absorber heat exchange (DAHX)

Implementing a second stage in the circuit is a way to keep the flexibility of the ACHP cycle and to increase the heat exchange at one time. This two-stage configuration was explored by Amrane and Rane (1991) [17] and is shown on Figure 7. In this configuration, the two stages exchange heat through a pair of absorber/desorber. A bleed line is used to compensate the eventual concentration difference between both stages. The lean solution from the low pressure side is connected to the rich solution of the high pressure circuit. This system can achieve temperature lift of up to 100 K with pressure ratio being 40% to 65% lower than then single stage configuration[17]. However, the capacity is reduced because both stages are supplied by the same compressor.

The last configuration uses a solution circuit and desorber/absorber heat exchange and was investigated by Groll and Radermacher (1994) [18] and is shown on Figure 8. In this system, the temperature intervals of desorber and absorber are increased which makes them overlap. Thanks to the internal heat exchange, the pressure ratio can be reduced by up to 75% for a temperature lift of 75 K compared to the single stage VCHP. Nevertheless, in this configuration, the pressure ratio is depending on the temperature glides inducing a flexibility loss.

Summary of the configurations

Configuration	Advantage	Disadvantage
Single-stage solution	Suitable for industrial applications, adjustable temperature glides and capacity	Overall performance is not optimal
Wet compression	Low discharge temperature and low required compressor work	Low flexibility
Two-stage solution circuit	High temperature lift	Small temperature glide
DAHX	High temperature glide	Low temperature lift

Table 1: Boons and banes of various cycle configurations

5.3.3 Compressor

Dano conducted a review on the different types of compressor on the market in a preliminary work leading to this report [2] (2022). The conclusion was that the screw compressor is the best kind of compressor for the following reasons for a use in a ACHP. Screw compressors are typically quieter and more efficient than other types of compressors, such as piston compressors. They can be either oil-lubricated or oil-free, depending on the application. They are typically more expensive than other types of compressors, but they offer many benefits, including reliability and durability.

In practice, it is not possible to achieve an ideal compression. Various volume and energy losses increase the power input needed for the compressor. :

Let us call V_{in} the working fluid flow at the entrance of the compressor. The stroke volume V_S of the compressor is then given by :

$$V_S = \frac{V_{in}}{\lambda} \tag{7}$$

With λ, the volumetric efficiency of the compressor.

Energy losses during the compression process make it polytropic rather than reversible adiabatic, which leads to a higher power consumption than the theoretical isentropic power. The isentropic efficiency (η_{is}) of the compressor is the ratio of the theoretical isentropic work (W_{is}) to the actual shaft work (W_{shaft}) of the compressor. These losses arise from various sources, such as heat exchange and fluid friction, which reduce the efficiency of the compressor and increase the power input needed to achieve the desired level of compression.

$$\eta_{is} = \frac{W_{is}}{W_{shaft}} \tag{8}$$

The screw compressor is the most important type of compressor used in industrial refrigeration. There are two main configurations of the screw compressor: the twin screw and the mono screw. In a twin screw compressor, the gas is compressed

by two intermeshing rotors, called the female rotor and the male rotor. In a mono screw compressor, there is only one rotor, but the gas is compressed by two intermeshing wheels. Lately, the mono screw compressor has not been able to increase its share of the market and it is used mostly in large air conditioning units for office buildings. The working area of the screw compressor is moving towards smaller capacities and operates with displacement lower than 100 m^3/h. Today, screw compressors are used in commercial systems or air conditioning systems and are available as hermetic, semi-hermetic or open compressors. In a screw compressor, the built-in ratio refers to the relationship between the volume of the air or gas being compressed and the volume of the compressor itself. The built-in ratio is determined by the design of the screw compressor, and it determines how much the air or gas is compressed.

$$\psi = \frac{V_1}{V_2} \tag{9}$$

The design of the screw compressor gives a constant volume ratio so the outlet pressure is given. In the design point, the discharge pressure of the compressor should be equal to the condenser/absorber pressure. As the condenser pressure is dependant on the temperature of the chilling media on the warm side, the pressure at the discharge of the compressor could be higher or lower than the condenser pressure. If the pressure in the condenser is lower that the discharge pressure, the compressor is over compressing. In this case, the compressor uses more energy than required. On the contrary, if the pressure in the condenser is higher than the discharge pressure, the gas will flow back and will need to be pushed again. This will also lead to an extra work of the compressor. That is why the efficiency of the compressor is at its maximum at the design point and will drop at different pressure ratio.

Challenges of compressors related to ACHP

As explained by Jensen (2015) [12], compressor is a major component of the ACHP as it sets limits to the achievable operation parameters. Different choices of compressor are possible which can lead to oil-free or oil lubricated solutions.

First, the compression mode must be chosen. As the temperature that are aimed at are high, positive displacement compressors like screw compressors and piston compressors offer promising solutions as they are able to achieve both high pressure ratios and small swept volume compared to dynamic compressors.
The most basic solution is to implement the compression thanks to one compressor stage. However, this can lead to very high discharge temperature that can cause damage to the components of the compressor but also deteriorate the lubricating oil. A few improvements are possible to make the discharge temperature lower like two-stage compression with intercooling or one stage compression with cooling and liquid injection. As shown by Ahrens et al. (2019) [8], for pressure levels of 2 bar and 20 bar, these two solutions can lower the discharge temperature from 270 °C for the one stage compression to 180 °C. The single-stage implementation has the lower installation costs but can lead to high discharge temperatures. Multi-stage compression allows intercoolings between the stage which lower the discharge temperature but leads to higher complexity. The liquid injection can allow oil-free operation but is also more complex than basic single-stage compression. According to Ahrens et al [19], the injection of lean solution reduces the exergy destruction rate and thus improve the overall system efficiency.

5.3.4 Absorber and Desorber

Ahrens et al (2018) [7] explains that the absorber is a major component of the ACHP system. The heat is transfered to the coolant through the absorber. Kang et al. [20] investigated two types of absorber : falling film and bubble type. The heat transfer surface must have a high area density and a good overall heat transfer coefficient in order to minimize the size of the heat exchanger. As the system under scrutiny is exchanging heat with a binary mixture which is ammonia-water, the heat transfer mode is of prime importance.
The two types of absorbers are shown on Figure 9. In both cases, ammonia-water liquid solution is flowing from the top to the bottom inside the heat exchanger. The vapor solution and the coolant are flowing the other way on both sides of the liquid. Thus, two counter current heat exchanges take place, one between the liquid

and vapor solution and the second between the liquid and the coolant which are separated by a carbon steel wall.

The two heat exchangers are different in the way the liquid and vapor are transferring the heat. According to Ahrens et al.[8], in the case of the falling film, the weak liquid solutions fall as a thin film on the wall while the ammonia vapor fills the free space and is absorbed while flowing upward. The driving force of this absoption is related to the vapour pressure and concentration and the mass transfer resistance. On the contrary, for the heat exchanger with the bubble absorption mode, the vapour is absorbed while bubbling into the liquid. In this case, the internal pressure inside the absorber is the main parameter which influences the temperature difference of the coolant.

Kang et al.[20] concludes that the bubble absorption mode heat exchanger can be 48,7% smaller compared to the falling film one because the absorption rate, heat transfer coefficient and mixing are better.

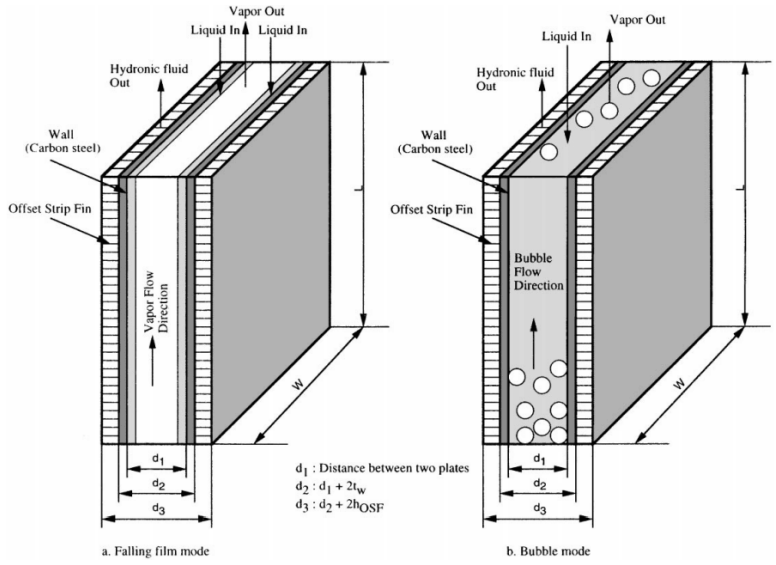

Figure 9: Diagram of plate heat exchangers with falling film and bubble absorption modes

5.3.5 Solution pump

Two main types of pumps are commercially available : the centrifugal pumps which move the fluid through a transfer of rotational energy from an impeller and the diaphragm pumps which are mainly used for small laboratory facilities. As mentionned above, the main challenge of this component is to avoid cavitation occuring when vapor bubbles are formed in the liquid flow. As the lean solution going through the pump is a saturated liquid, a small variation in the operational speed of the solution pump can cause a state change. According to Ahrens (2023) [10], there are two main principles to avoid cavitation. The first one is to reduce pressure losses in the pump inlet line to keep the solution in the liquid state. The second solution is to operate smooth variation of the pump and compressor´s speed. Markmann et al. (2019) [21] described a way to stabilize the low-pressure level in the separator. The expansion valve's opening degree is used to regulate the liquid level in the high-pressure receiver and reduce the rapid pressure changes. Amrane et al. (1991) [22] investigated another solution to limit cavitation using an external heat exchanger. The lean solution is subcooled through a tube-in-tube heat exchanger in order to minimise the pressure losses.

6 Methods

6.1 Experimental

6.1.1 The Experimental ACHP Prototype

In order to look into the performance of the ACHP system, an experimental prototype named "Osenbrück 4.0 Heat Pump" was built in a NTNU lab based on the model presented on Figure 4. The system is designed for a maximum heat capacity of 200 kW with a maximum operating pressure of 40 bar and an operational temperature range from -10 °C to 190 °C. An auxiliary system provides the required heat source and heat sink water circuits. The facility is shown on Figure 10.

Figure 10: ACHP prototype of the NTNU lab

Characteristics of the facility

The components are designed in order to resist high temperatures and pressures

and are able to provide the expected outlet sink temperature. Parameters such as the weak solution composition, the heat source temperature or heat sink temperature are controllable. Also, as the objective is to test a large range of operating conditions, the sensors and auxiliary equipment are able to cover it. The mass and energy flow are relatively small compared to an actual industrial heat pump. Moreover, as the working fluid is an ammonia-water mixture, the compatibility of the equipment has been verified beforehand. Ammonia and hydrous ammonia is compatible with iron, steel, stainless steel and aluminum. Materials such as copper, zinc and copper-based alloys must be avoided because of corrosion problems (Stene J.).[23]

The facility system is based on a single-stage solution circuit with an internal heat exchanger between the lean and the rich solutions.

Design of the compressor

The compressor is designed to receive inlet temperature in the range 50°C - 70 °C and pressure between 3 and 5 bar. The water content in the ammonia vapor is expected to be between 2% and 5%. The mass flow through the compressor must be as small as possible for the laboratory scale. The compression is oil-free in order to reduce the cost and complexity of the facility and is done in one step only. Liquid injection is used in the compressor to lower the discharge temperature and lubricate and seal the screws. This injection is realized with the lean solution downstream of the solution pump. The discharge pressure is expected to be higher than 20 bar in order to reach high sink outlet temperatures. The compressor model chosen for the facility is the MYCOM screw i125 L-M which is a twin-screw compressor. The volumetric ratio of the compressor is 3.65 and the maximum discharge temperature is 180 °C. The maximum operation speed is 3600 rpm for which the swept volume is 350 m^3/h. The lean solution is injected in three different locations of the compressor. The main injection port provides all bearings with liquid and inject the lean solution into the compression chamber at the beginning of the compression process. Two other injection ports are put at the end of the compression phase, feeding the solution in the male and female rotor cavities. The mass flow rate of the injected solution can be regulated thanks to valves for every port. A picture of the compressor is shown on Figure 11.

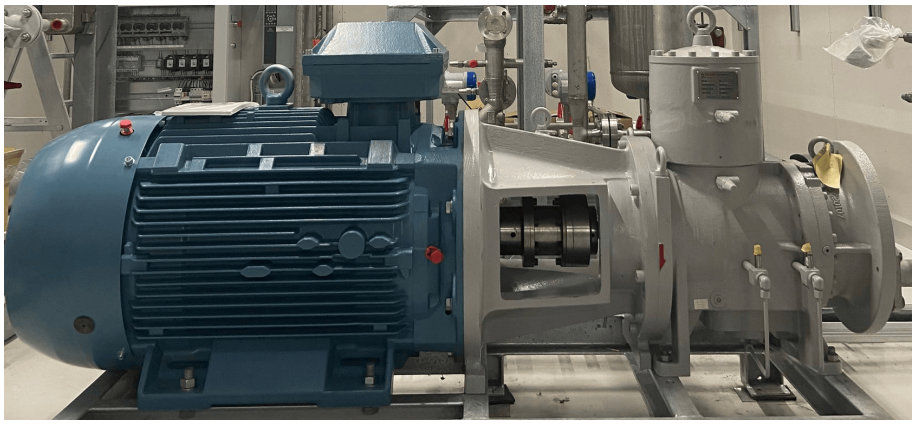

Figure 11: Compressor of the NTNU facility

Injection line

Ahrens et al. [24] investigated numerically the possibilities concerning oil-free liquid injected screw compressor in ACHP. They discussed the effects of varying the NH_3 fraction of the injected solution, the injected mass flow rate and the position of the injection. There are two ways of arranging the injection line: either from the rich solution which has a fraction of ammonia around 0.7 or from the lean solution which has a fraction of ammonia of around 0.4. Ahrens demonstrates that the lower the ammonia fraction injected, the lower the discharge temperature. Besides, increasing the mass flow rate injected leads to lower discharge temperature, pressure and compression power. This first preliminary analysis shows that absorption and desorption are both achievable during the compression process with liquid injection. Injection with a solution with a low concentration of NH_3 should be performed in order to decrease the discharge temperature and the compression power. To ensure a continuous lubrication during the compression process, the injection rate must be around 10 % of the suction mass flow rate at the inlet of the compressor.

As shown on Figure 12, the compressor of the facility is manufactured with three injection ports. The main injection port is supplying lean solution on the bearings and into the compression chamber at the start of the compression process. At the end of the compression process, two more ports are placed in order to inject liquid in the male and female rotor cavities. The total injection mass flow rate and each of the specific ones can be controlled independently thanks to flow setting valve during operation.

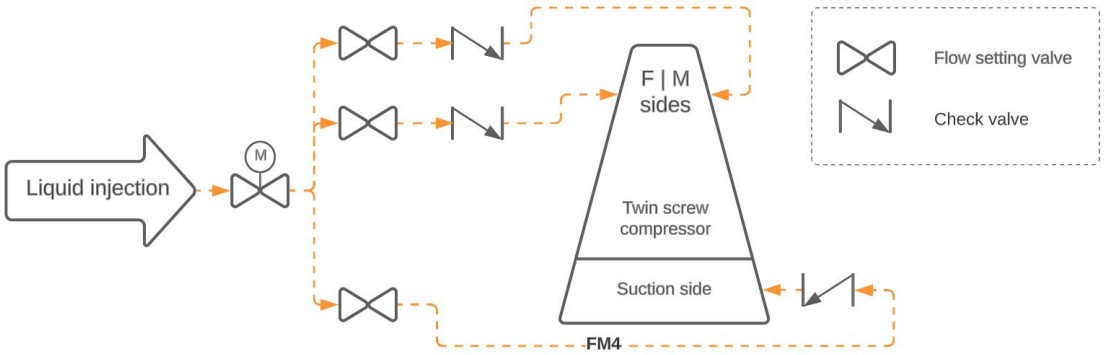

Figure 12: Schematic of the compressor section with liquid injection line

Design of the heat exchangers

The heat exchangers of the facility are plate heat exchangers manufactured by Alfa Laval AS. The characteristics of the heat exchangers are listed Table 2 :

	Desorber	Absorber	IHX
Number of plates	40	40	20
Length (m)	0.9	0.9	0.25
Width (m)	0.111	0.111	0.111
Corrugation angle (°)	50	65	65
Wall thickness (m)	0.0004	0.0004	0.0004
Pattern amplitude (m)	0.002	0.002	0.002
Pattern wave length (m)	0.007	0.007	0.007

Table 2: Characteristics of the heat exchangers of the facility

Receiver and separator

The liquid-vapor separator is used to divide both phases of the rich solution. The gaseous outlet of the separator enters the compressor and the liquid phase goes through the solution pump. The separator is used as a buffer tank in the facility. A high-pressure receiver is put between the absorber and the IHX to ensure that only liquid solution enters the IHX. This secures a high heat transfer rate. The liquid level in the high-pressure receiver can be controlled allowing to modify the operating

conditions of the ACHP.A picture of the liquid-vapor separator is shown on Figure 13.

Figure 13: Liquid-vapor separator of the NTNU facility

Solution pump

The solution pump is placed between the separator and the high-pressure side of the facility. The pump must deliver a pressure ratio high enough so that the pressure losses in the mixing section and the IHX are compensated. The pump was chosen to be able to resist to the corrosion of the ammonia-water mixture. The selected pump is a multistage, centrifugal pump of type CRN 3-31 S-FGJT-E-HQQE equipped with a controlled motor manufactured by Grundfos. The pump can deliver volumes flow from 0 to 4.5 m^3/h. The maximum operating pressure is 50 bar and the maximum solution temperature is 120 °C which is significantly higher than the operating conditions. The volume flow of the pump can be regulated thanks to a frequency converter of type FC202 – 3 kW manufactured by Danfoss A/S.

Since the mixture is at vapor-liquid in the separator, an increase of the compressor speed leading to a pressure drop will cause desorption of ammonia from

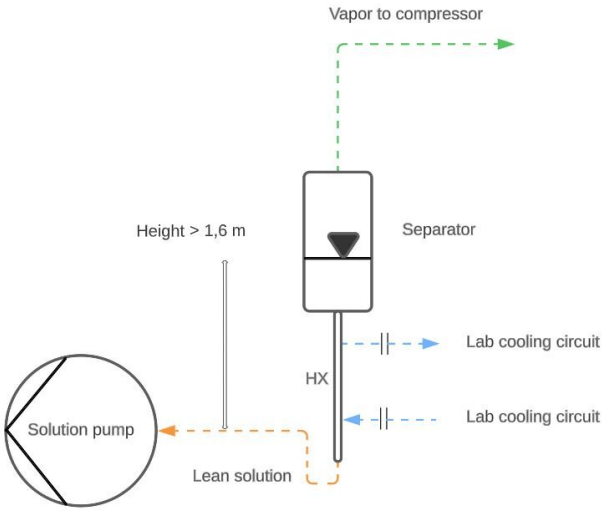

Figure 14: Tube-in-tube heat exchanger at the intake of the solution pump

the liquid phase. Thus, vapor will be formed and the liquid flow to the solution pump will decrease or cavitation can occur. In order to avoid these problems in the solution pump, the intake pipe is designed as a heat exchanger. The lean solution flowing out the separator can be subcooled thanks to an external cooling circuit as shown on Figure 14. The liquid column after the liquid separator is superior to 1.6 m which ensure a sufficient upstream pressure into the solution pump and prevents the formation of vapor.

Expansion valve

The expansion valve selected for the facility is the ICM 20A associated with an ICAD 600A actuator. The valve is placed downstream of the IHX and ensure reduction of the pressure associated with a temperature diminution upstream of the desorber. The expansion is almost isenthalpic. The high pressure level is controlled thanks to the opening degree of the valve.

Auxiliary system

The lab rig has been functional from November 2022 and tests started to be done. The main objective was to try to set the parameters of the cycle in order to obtain a steady state. Unfortunately, the seal of the shaft broke in March which stopped the experiments during a few months. As a result this report will not present the operating parameters leading to a steady state but the performances of

the components during the test runs done. The analysis of a set of data collected on 27th February will be conducted in the following part of the report.

6.2 Numerical

The numerical modelling of the ACHP was done thanks to Dymola (Dynamic Modelling Library, version 2022, Dassault systems) using Modelica langage. Modelica is an open object oriented Equation based programming language for modelling of complex physical systems including electrical, mechanical and thermophysical subcomponents. The structure is object oriented and allows reuse of developed components, such as compressors, heat exchangers or valves. The model was done using two commercial Modelica libraries : TIL-suite 3.10.0 and TILMedia 3.10.0 provided by TLK-Thermo GmbH. The objective of the simulation is to model the "Osenbrück 4.0 Heat pump" facility of NTNU as precisely as possible and define the optimal operating parameters. Dymola has a graphical interface and a programming interface, allowing users to either arrange components and input parameters visually or to alter the programming code directly.
As explained in section 2, the objective of the numerical simulation is to be able to predict the behavior of the experimental cycle and to get comparable results. As a result, the parameters chosen for the numerical modeling must be as close as possible to the actual operating variables.
The simulated cycle is for the most part the one shown on Figure 4. A few assumptions were made to simplify the simulation :

- The pressure drop created by frictions in the pipes and components and the heat losses to the surroundings are neglected.
- Upstream of the absorber, the mixing of the lean solution from the IHX and the vapor from the compressor is assumed adiabatic.
- The liquid and vapor phases are assumed at thermodynamic equilibrium in the liquid-vapor separator.

- As the high-pressure receiver does not contribute thermodynamically to the system, it was neglected due to the lack of a relevant model in TIL library.

The components of the cycle and their settings were defined as following :

6.2.1 Compressor

Model : Efficiency based compressor model (VLEFluids components)
Volumetric efficiency : 0.6
Isentropic efficiency : 0.6
In the model with intercooling, a proportionnal-integral controller is used to set the intermediate pressure. In that case, the intermediate pressure p_{int} is defined as :

$$p_{int} = \sqrt{p_{LP} \cdot p_{HP}} \tag{10}$$

with p_{LP} the low pressure and p_{HP} the high pressure.

6.2.2 Heat exchangers

Determination of the heat transfer coefficients

An important parameter of the heat exchangers is the heat transfer coefficient α. This coefficient is dependant on multiple parameters and has to be calculated for the absorber, the desorber and the IHX on both sides.

Single phase heat transfer

In case of a single phase heat transfer, Martin´s correlation [25] (1996) can be used. Martin found a semi-empirical correlation based on an analogy to friction. The Moody friction factor is calculated thanks to Equation (11)

$$\frac{1}{\xi} = \frac{\cos(\varphi)}{\sqrt{0.18\tan(\varphi) + 0.36\sin(\varphi) + \frac{\xi_0}{\cos(\varphi)}}} + \frac{1-\cos(\varphi)}{\sqrt{3.8\xi_{1.0}}} \tag{11}$$

In Equation (11), φ is the corrugation inclination angle ($\varphi = 90° - \beta$). Further, ξ_0 and $\xi_{1.0}$ are the friction factors for straight longitudinal flow ($\varphi = 0°$) and wavy longitudinal flow ($\varphi = 90°$) respectively. The value of these friction factors depend on the flow. If the flow is laminar ($\mathrm{Re}/\phi < 2000$) : ξ_0 and $\xi_{1.0}$ can be found by Equation (12) and (13).

$$\xi_0 = \frac{64\varphi}{Re} \tag{12}$$

$$\xi_{1.0} = \frac{597\varphi}{Re} + 3.85 \tag{13}$$

If the flow is turbulent ($\mathrm{Re}/\phi > 2000$) : ξ_0 and $\xi_{1.0}$ can be found by Equation (14) and (15).

$$\xi_0 = (1.8 \log_{10} \frac{Re}{\varphi} - 1.5)^{-2} \tag{14}$$

$$\xi_{1.0} = \frac{39}{(Re/\varphi)^{0.289}} \tag{15}$$

Then the Nusselt number of the flow is determined thanks to Equation (16).

$$Nu = \Phi \cdot 0.122 \cdot Pr^{1/3} \cdot (\frac{\eta}{\eta_w})^{1/6} (\xi \cdot (\frac{Re}{\varphi})^2 \cdot \sin(2\varphi))^{0.374} \tag{16}$$

Where η is the dynamic viscosity of the flow and η_w is evaluated at the exchanger surface temperature. Pr is the Prandtl number derived from the specific heat cp, the viscosity η and the thermal conductivity λ. The Reynolds number is calculated thanks to the mass flux G and the hydraulic diamater assumed to be two times the depth of the plate : Dh=2b.
The cross sectional area used for the mass flux is calculated as $Across = Nch \cdot W \cdot b$ with Nch=Nplates-1 (number of channels) and W the width of the plates.

Finally, Equation (17) gives the relation between the Nusselt number and the heat transfer coefficient.

$$\alpha = \frac{Nu \cdot \lambda}{Dh} \tag{17}$$

Desorption

Taboas et al. investigated the thermal characteristics of a two-phase ammonia-water mixture in plate heat exchanger during desorption [26] (2012). They derived a correlation based on a transition criterion to assess wether the desorption is dominated by nucleate or convective flow boiling. The criterion is based on the calculation of vapour and liquid velocities in the mixture that are calculated like in Equation (18) and (19).

$$u_{SL} = \frac{G(1-q)}{\rho_l} \tag{18}$$

$$u_{SV} = \frac{G \cdot q}{\rho_v} \tag{19}$$

with q, the quality of the mixture and ρ, the density for vapor (subscript v) and liquid (subscript l).

$$u_{SV} < 111.88 u_{SL} + 11.848 \ [m/s] \tag{20}$$

If the inequality (21) is satisfied, then :

$$u_{SV} < 111.88 u_{SL} + 11.848 [m/s] \tag{21}$$

$$\alpha = 5 Bo^{0.15} \cdot \alpha_{lo} \tag{22}$$

$$Bo = \frac{q''}{G \cdot hlv} \tag{23}$$

With q" , the heat flux of the exchanger and Bo, the boiling number. Here, α_{lo} is the liquid only heat transfer coefficient calculated with Martin´s correlation.

If the inequality (21) is not satisfied, then :

$$\alpha = \max(F \cdot \alpha_{lo},\ 5Bo^{0.15} \cdot \alpha_{lo}) \tag{24}$$

$$F = (1 + \frac{3}{X_{tt}} + \frac{1}{X_{tt}^2})^{0.2} \tag{25}$$

$$X_{tt} = (\frac{\eta_l}{\eta_v})^{0.1}(\frac{1-q}{q})^{0.9}(\frac{\rho_v}{\rho_l})^{0.5} \tag{26}$$

Where F is the Chisholm´s two-phase enhancement factor and X_{tt} is the Lockhartt-Martinelli factor.

Absorption

To calculate the heat transfer coefficient of the ammonia-water mixture in the absorber, the Silver/Bell-Ghaly method can be used [27] (1947), [28] (1972). This method states that the heat transfer coefficient can be derived from the vapor and condensate layer heat transfer coefficients and a correcting factor called Z as in Equation (27).

$$\alpha = (\frac{1}{\alpha_{lo}} + \frac{Z}{\alpha_{vo}})^{-1} \tag{27}$$

$$Nu_{lo} = 4.188 Re_{lo}^{0.4} \cdot Pr_l^{1/3} \tag{28}$$

Where α_{vo} is the vapor only heat transfer coefficient calculated from Martin´s correlation. α_{lo} is the condensate layer heat transfer coefficient corrected for two-phase flow effects.
The Z factor is calculated from Equation (29).

$$Z = q \cdot c_{p,v} \cdot \frac{dT}{dh} \tag{29}$$

Where q is the vapor mass fraction, $c_{p,v}$ is the specific heat of the vapor phase and dT/dh is the gradient of the equilibrium absorption curve.

Calculation of the heat transfer coefficients

Table 3 is a summary of the method used to calculate the heat transfer coefficients for each exchanger.

	Water side	**Mixture side**
Desorber	Martin (1996)	Taboas et al. (2012) and Martin (1996) for the liquid phase
Absorber	Martin (1996)	Bell (1972) and Silver (1947) with Martin (1996) for vapor phase heat transfer
	Rich solution	**Lean solution**
IHX	Martin(1996)	Martin (1996)

Table 3: Summary of the methods used to determine the heat transfer coefficients

Table 4 is a summary of the calculated values for the heat transfer coefficients.

	Water side	**Mixture side**
Desorber	$\alpha = 925\ Wm^{-2}K$	$\alpha = 2740\ Wm^{-2}K$
Absorber	$\alpha = 886\ Wm^{-2}K$	$\alpha = 1030\ Wm^{-2}K$
	Rich solution	**Lean solution**
IHX	$\alpha = 1300\ Wm^{-2}K$	$\alpha = 1240\ Wm^{-2}K$

Table 4: Summary of the heat transfer coefficient values

Absorber, desorber and IHX

Model : Plate vle fluid liquid parallel flow HX (VLEFluidLiquid) for the absorber and desorber.

Model : Plate vle fluid fluid parallel flow HX (VLEFluidFluid) for the IHX.

The characteristics of the heat exchangers are as defined in Table 2.

In each heat exchanger, a constant value of α is considered for the heat transfer coefficient and the pressure drop are neglected. As mentionned in table 4, the heat transfer coefficients are not the same on the water side and on the mixture side. In the cycle, two absorbers and two desorbers are placed in series and their thermal and geometric characteristics are considered exactly the same.

Expansion valve

Model : Orifice valve

The effective flow area of the valve is defined by input. This means that a PI controller is used in order to regulate the effective flow area of the valve depending on the downstream pressure. This is made to stabilize the low pressure in the cycle. The characteristics of the PI controller such as the proportionnal gain K and the time constant Ti have to be set afterward so it converges.

Liquid-vapor separator

Model : Separator (TIL VLEfluid)

The volume of the separator is set to a value between 0.001 and 0.1 m^3 and is the real value of the facility. This leads to the same steady state. The initial filling level is set to 0.5.

Solution pump

Model : Simple pump (TIL VLEfluid)

The preset variable of the solution pump is the mass flow. This means that the mass flow through the pump is constant at all time. The pump efficiency is set to 0.4.

6.2.3 Initial conditions

The initial conditions of the cycle have to be set precisely in the software. The calculations on Dymola are very sensitive about the initial state. Here is the procedure that was used to set these initial conditions :

- Set the ammonia-water ratio of the cycle.
- Choose the low pressure and the high pressure levels. Set the sink and absorber inlet and outlet temperature. Set the sink mass flow and calculate the heating capacity of the sink given in Equation (30) :

$$Q_{sink} = \dot{m}_{sink} \cdot cp_{eau} \cdot \Delta T_{sink} \tag{30}$$

  Where Q_{sink} (W) is the heat load of the sink, and ΔT_{sink} is the temperature difference between the outlet and the inlet of the sink.

- Thanks to the ammonia-water ratio, the temperature and the pressure level, the enthalpies can be calculated at the inlet and outlet of the absorber thanks to REFPROP. Thus, the mass flow rate of the rich solution can be derived from Equation (31) :

$$\dot{m}_{rich} = \frac{Q_{sink}}{h_{inlet,abs} - h_{outlet,abs}} \tag{31}$$

- In the desorber, the source inlet and outlet temperature are also set as well as the mass flow rate. Thus, the cooling capacity is calculated with the same Equation than (30). The outlet temperature of the desorber is also set.
- As the pressure, the temperature and the composition of the mixture are known in the liquid-vapor separator, it is possible to calculate the quality thanks to REFPROP. The circulation ratio is derived from the quality based on Equation (32) :

$$CR = 1 - q_{separator} \tag{32}$$

- As a result, the lean solution mass flow rate can be calculated from Equation (1) and the mass flows are knows at all points in the cycle.
- The pressure, temperature and ratio are known at all points in the cycle and the associated enthalpies can be derived from it with REFPROP. Thus, all the characteristics can be put in the components settings. For the heat exchangers, the initialization is based upon a linear enthalpy distribution.
- After the compressor speed is set, the displacement can be derived from Equation (33) :

$$d = \frac{V_S}{N} \tag{33}$$

Where V_s $(m^3.s^{-1})$ is the stroke volume from the compressor derived from Equation (7) and N is the speed of the compressor (Hz). d is the displacement of the compressor in m^3.

6.2.4 Cycle simulation

no IHX, IHX, intercooling ...

The COP of the cycle is calculated thanks to Equation (34) :

$$COP = \frac{Q_{sink}}{W_{comp} + W_{pump}} \tag{34}$$

Where W_{comp} (kW) is the shaft power of the compressor and W_{pump} (kW) is the shaft power of the solution pump.

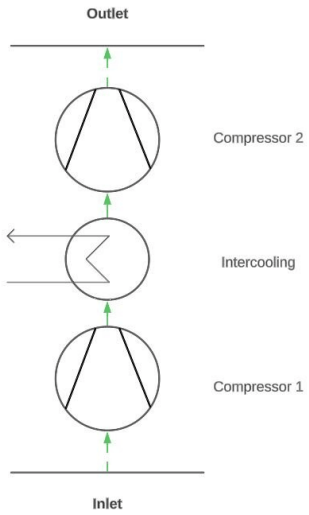

Figure 15: Compressor configuration with intercooling

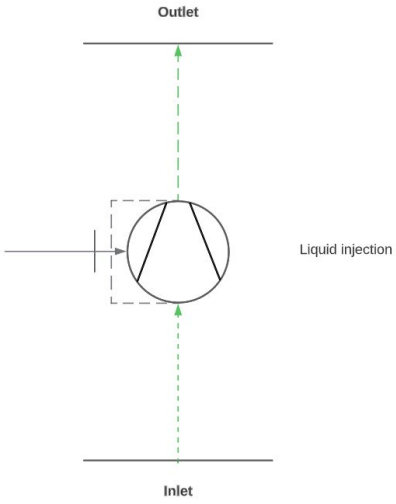

Figure 16: Compressor configuration with direct injection

7 Results

All the indices of this section are based on the number given of figure 17.

7.1 Experimental

Here are the parameters of the test :

- **Global ammonia-water ratio** : 50/50
- **Sink mass flow** : 0.5 kg/s
- **Source mass flow** : 0.5 kg/s

All the other variables measured will be averaged on a time period of one minute as the regime is not perfectly stable.

The following table presents the pressure and temperature state in the cycle :

Three flow meters are placed in the cycle in order to measure the mass flow rate at different positions as shown on Figure 18.

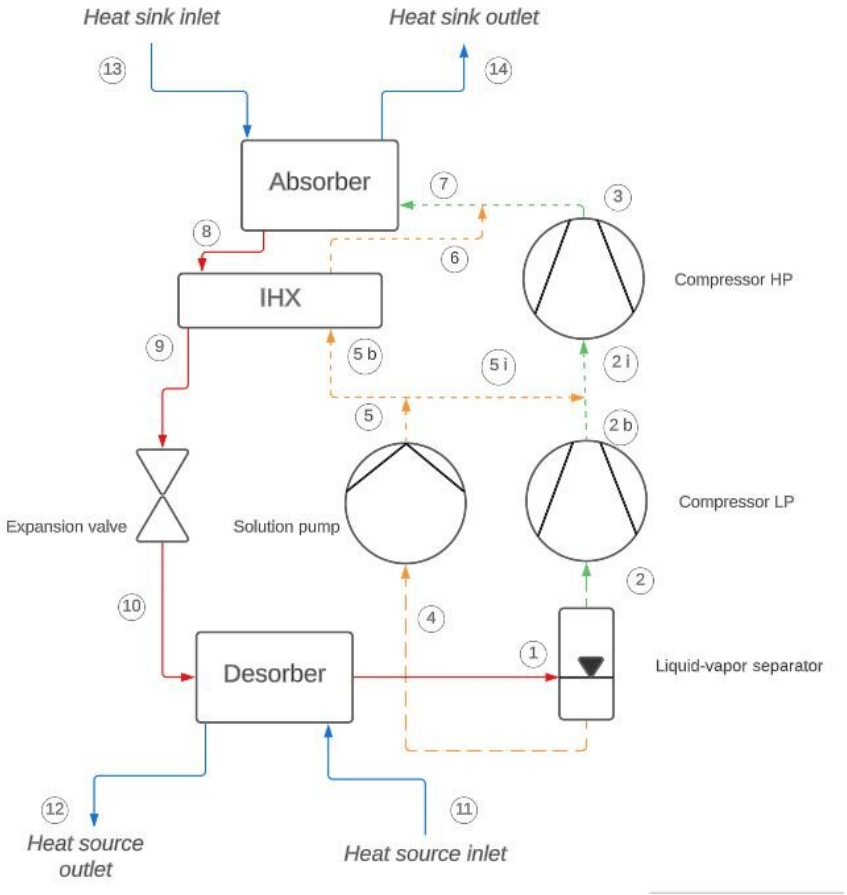

Figure 17: Cycle with reference state point numbers

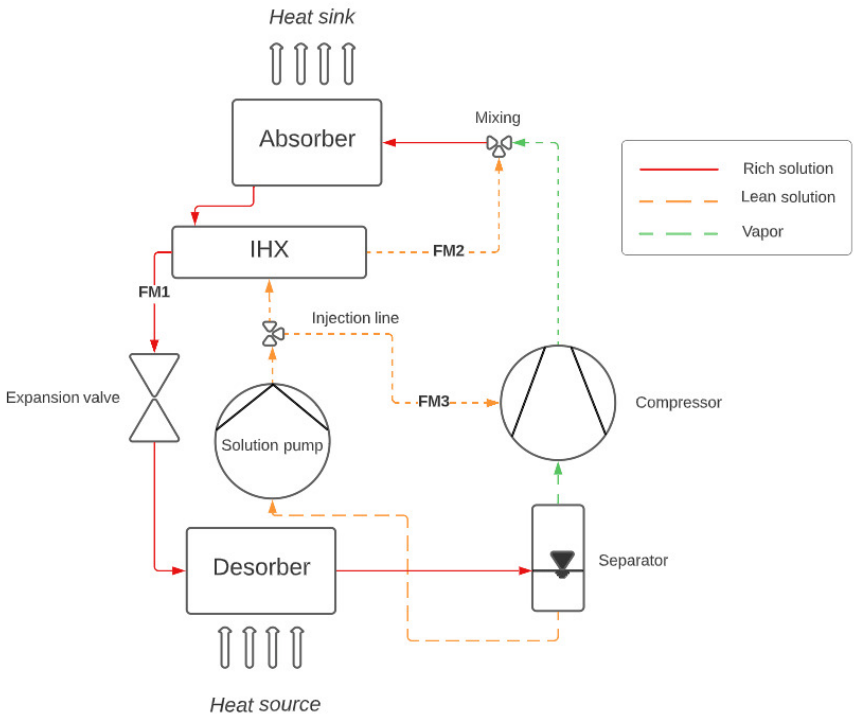

Figure 18: Flow meters of the experimental cycle

State point	Temperature (°C)	Pressure (bar)
Suction compressor	68.8	7.6
Discharge compressor	103.1	16.9
Injection line	70.6	7.9
Outlet IHX lean solution	82.0	16.9
Inlet absorber	98.5	16.8
Outlet absorber	88.4	16.7
Inlet valve	81.1	16.9
Inlet desorber	68.3	7.8
Outlet desorber	71.5	7.6
Inlet sink	83.7	1
Outlet sink	97.9	1
Inlet source	77.1	1
Outlet source	68.6	1

Table 5: Temperatures and pressures in the cycle during the test

- **FM1 = 0.27 kg/s** : mass flow rate of the rich solution out of the internal heat exchanger.
- **FM2 = 0.17 kg/s** : mass flow rate of the lean solution out of the internal heat exchanger.
- **FM3 = 0.075 kg/s** : mass flow rate of the injected solution into the compressor.

Hence, using (1) :

$$CR = \frac{FM2}{FM1} = 0.63 \tag{35}$$

The theoretical limit value of the coefficient of performance is given by COP_{Lorenz}

Thus, using Equation (5) :

$$T_{log,mean,sink} = 90.6 \tag{36}$$

$$T_{log,mean,source} = 72.8 \tag{37}$$

Also, using Equation (4) :

$$COP_{Lorenz} = 5.1 \tag{38}$$

7.1.1 Compressor

As the lean solution is injected into the compressor, the inlet and outlet mass flow rates are different :

$$Compressor_{inlet,flow} = FM1 - FM2 - FM3 = 0.024\ kg/s \tag{39}$$

$$Compressor_{outlet,flow} = FM1 - FM2 = 0.1\ kg/s \tag{40}$$

Using equation (7), the volumetric efficiency is given by :

$$\lambda = \frac{V_{in}}{V_S} \tag{41}$$

$$\lambda = \frac{Compressor_{inlet,flow} \cdot v_{inlet}}{V_S} \tag{42}$$

where v is the compressor inlet mass density.

Using the software REFPROP for the thermodynamic calculations and assuming an ammonia-water ratio of 98/2 at the inlet of the compressor :
$v_{inlet} = 0.21\ m^3/kg$

The compressor has a stroke volume of 139 m^3/h at a speed of 1410 rpm according to the manufacturer.

Finally :

$$\lambda = \frac{0.024 \cdot 0.13}{139/3600} = 0.13 \tag{43}$$

The volumetric efficiency is very low. This is expectable as the injected mass flow rate is more than 3 times bigger than the inlet mass flow rate of the compressor.

7.1.2 Absorber

In this subsection, a performance analysis of the absorber is conducted using the effectiveness NTU-method. This method is a way to evaluate the performance of a heat exchanger thanks to the ratio between the actual heat exchange that takes place and the maximum achievable heat transfer possible at the temperature involved.

The heating capacity of the sink can be calculated from the enthalpy difference between the inlet and the outlet of the sink. It can also be calculated on the mixture side as the heat received is equal to the heat transfered when the steady state is reached.

Using REFPROP :

$h_{inlet,sink} = 351.2\ kJ/kg$

$h_{outlet,sink} = 410.1\ kJ/kg$

$h_{outlet,absorber} = 337,3\ kJ/kg$

$h_{inlet,absorber} = 527,2\ kJ/kg$

The heating capacity is calculated as following :

$$Q_{sink} = \dot{m}_{water} \cdot (h_{outlet,sink} - h_{inlet,sink}) = 29.4\ kW \tag{44}$$

In the steady state, this value should be equal to :

$$Q_{sink,mixture,side} = \dot{m}_{mixture} \cdot (h_{inlet,absorber} - h_{outlet,absorber}) = 51.3\ kW \tag{45}$$

The fact that these two values are different shows that the steady state has not

been reached. All the heat provided by the mixture is not transfered to the water on the sink side.

The maximum heat transfer is given by :

$$Q_{max} = Cp_{min} \cdot (T_{inlet,sink} - T_7) \tag{46}$$

Where $Cp_{min} = min\ |Cp_{water} \cdot \dot{m}_{water}, Cp_{mixture} \cdot \dot{m}_{mixture}|$

$Cp_{water} \cdot \dot{m}_{water} = 4.20 \cdot 0.5 = 2.1\ kW/K$

$Cp_{mixture} \cdot \dot{m}_{mixture} = 4.8 \cdot 0.27 = 1.29\ kW/K$

$Cp_{min} = 1.29\ kW/K$

The cycle points are numbered on Figure 17.

$T_{inlet,sink} = 83.7\ \ ^{\circ}\mathrm{C}$

$T_7 = 98.5\ \ ^{\circ}\mathrm{C}$

$$Q_{max} = 19.1\ kW \tag{47}$$

$$\epsilon_{absorber} = \frac{Q_{sink}}{Q_{max}} \tag{48}$$

As the efficiency would be superior to 1, it makes no sense to calculate it. A test run in the steady state would make possible to calculate the efficiency.

7.1.3 Desorber

The cooling capacity of the desorber can be calculated the same way using the source inlet and outlet enthalpies. Using REFPROP :

$h_{inlet,source} = 322.7\ kJ/kg$

$h_{outlet,source} = 287.4\ kJ/kg$

$h_{outlet,desorber} = 430\ kJ/kg$

$h_{inlet,desorber} = 486\ kJ/kg$

The cooling capacity is calculated as following :

$$Q_{source} = \dot{m}_{water} \cdot (h_{inlet} - h_{outlet}) = 17.64\ kW \tag{49}$$

The same way, the heat transfer provided by the mixture is given by :

$$Q_{source,mixture,side} = \dot{m}_{mixture} \cdot (h_{outlet,desorber} - h_{inlet,desorber}) = 15.1\ kW \tag{50}$$

Here, as the heat transfer received by the mixture is almost equal to the one transfered from the source (86%), the steady state is almost reached. The calculation of the efficiency might be more accurate. The maximum heat transfer is given by :

$$Q_{max} = Cp_{min} \cdot \dot{m}_{mixture} \cdot (T_{inlet,source} - T_{10}) \tag{51}$$

Where $Cp_{min} = min\ |Cp_{water} \cdot \dot{m}_{water}, Cp_{mixture} \cdot \dot{m}_{mixture}|$

$Cp_{water} \cdot \dot{m}_{water} = 4.19 \cdot 0.5 = 2.1\ kW/K$

$Cp_{mixture} \cdot \dot{m}_{mixture} = 4.6 \cdot 0.27 = 1.24\ kW/K$

$Cp_{min} = 1.24\ kW/K$

The cycle points are numbered on Figure 4.

$T_{inlet,source} = 77.1\ \ ^{\circ}\text{C}$

$T_{10} = 68.3\ \ ^{\circ}\text{C}$

$$Q_{max} = 12.3\ kW \tag{52}$$

$$\epsilon_{absorber} = \frac{Q_{source}}{Q_{max}} \tag{53}$$

Once again, this efficiency would be superior to 1. The conclusion is the same than for the absorber.

7.1.4 General performance of the cycle

During the test, the compressor has a shaft work of $W_{comp} = 11.8\ kW$ and the pump consumes a power of $W_{pump} = 0.7\ kW$. Also, $Q_{sink} = 29.4\ kW$ as calculated previously.

Using Equation (34), the COP can be calculated :

$$COP = \frac{29.4}{11.8 + 0.7} = 2.35 \tag{54}$$

Thus, thanks to Equation (6),

$$\eta_{Lorenz} = \frac{COP}{COP_{Lorenz}} = \frac{2.35}{5.1} = 0.46 \tag{55}$$

Nevertheless, as mentionned before, the heat load calculated is not from a steady state which means its value is not accurate. Usually a COP is calculated in the steady state. That is why the value found has to be considered carefully.

7.2 Numerical

7.2.1 Dymola simulation

7.2.1.1 Cycle without injection and internal heat exchanger

This paragraph is based on the cycle shown on Figure 27.

Temperature, pressure and mass flow in the cycle

The most simple simulation has been done without the IHX and the injection line. This means that refering to Figure 17, point 5 = point 5b = point 5i and point 2/2b/2i. Besides, point 6 = point 5 and point 9 = point 8.

The initial conditions of the cycle were determined thanks to the procedure described in section 4. The simulation converges toward a steady state which is

reached after around 150 seconds.

Table 6 presents the results of the simulation.

State point	Mass flow rate (kg/s)	Water mass fraction	Temperature (°C)	Pressure (bar)
1	0.138	0.35	59.1	5
2	0.061	0.02	59.1	5
3	0.061	0.02	250.2	21
4	0.077	0.62	59.1	5
5	0.077	0.62	59.8	21
7	0.138	0.35	114	21
8	0.138	0.35	82.4	21
10	0.138	0.35	39	5
11	0.5	1	65	1
12	0.5	1	45.7	1
13	0.5	1	65	1
14	0.5	1	97.2	1

Table 6: Simulation results of the cycle without injection nor IHX

Performance of the cycle

The characteristics of the cycle when the steady state is reached are as following :

- Rich solution water ratio : 0.35
- Lean solution water ratio : 0.62
- $Q_{Absorber,1}$: 32.6 kW
- $Q_{Absorber,2}$: 34.9 kW
- $Q_{sink} = Q_{Absorber,1} + Q_{Absorber,2}$: 67.5 kW
- $Q_{Desorber,1}$: 21.1 kW

- $Q_{Desorber,2}$: 19.1 kW
- $Q_{source} = Q_{Desorber,1} + Q_{Desorber,2}$: 40.2 kW
- Compressor speed : 50 Hz
- W_{comp} : 23.1 kW
- W_{pump} : 0.37 kW
- Circulation ratio : 56 %

The COP can be derived from Equation (34) :

$$COP = \frac{67.5}{23.1 + 0.37} = 2.88 \tag{56}$$

7.2.1.2 Cycle without injection and with internal heat exchanger

This paragraph is based on the cycle shown on Figure 28.

Temperature, pressure and mass flow in the cycle

Running the simulation with the internal heat exchanger added let us evaluate the contribution of it.

The same parameters than previously are applied to the simulation which runs with the cycle shown on Figure 4. The simulation converges toward the steady state after around 200 seconds.

As there is no injection line, refering to Figure 17, point 5 = point 5b = point 5i and point 2/2b/2i.

Table 7 presents the results of the simulation.

Performance of the cycle

The characteristics of the cycle when the steady state is reached are as following :

State point	Mass flow rate (kg/s)	Water mass fraction	Temperature (°C)	Pressure (bar)
1	0.138	0.35	57.8	5
2	0.062	0.02	57.8	5
3	0.062	0.02	**284**	27
4	0.077	0.61	57.7	5
5	0.077	0.61	58.8	27
6	0.077	0.61	67.7	27
7	0.139	0.35	125,9	27
8	0.139	0.35	87.6	27
9	0.139	0.35	69.9	27
10	0.139	0.35	27.1	5
11	0.5	1	65	1
12	0.5	1	29.7	1
13	0.5	1	65	1
14	0.5	1	115	1

Table 7: Simulation results of the cycle without injection and with the IHX

- Rich solution water ratio : 0.35
- Lean solution water ratio : 0.61
- $Q_{Absorber,1}$: 59.7 kW
- $Q_{Absorber,2}$: 47.0 kW
- $Q_{sink} = Q_{Absorber,1} + Q_{Absorber,2}$: 106.7 kW
- $Q_{Desorber,1}$: 27.6 kW
- $Q_{Desorber,2}$: 46.0 kW
- $Q_{source} = Q_{Desorber,1} + Q_{Desorber,2}$: 73.6 kW
- Q_{IHX} : 3.2 kW

- Compressor speed : 50 Hz
- W_{comp} : 27.9 kW
- W_{pump} : 0.50 kW
- Circulation ratio : 56 %

The COP can be derived from Equation (34) :

$$COP = \frac{106.5}{27.6 + 0.5} = 3.79 \tag{57}$$

7.2.1.3 Cycle with the injection line

This paragraph is based on the cycle shown on Figure 29.

Temperature, pressure and mass flow in the cycle

The cycle is run with the injection done as shown on Figure 19. It is not possible to inject the solution directly into the compressor as shown on Figure 16 because the component does not allow it on Dymola. It would have been possible to simulate the cycle as shown on Figure 15 in which the lean solution is not mixed directly and the heat transfers trough an exchanger. Neverteless, in the actual facility of NTNU, the injected lean solution is mixed with the vapor in the compressor so it is more accurate to model it like on Figure 19. Instead, the compressor is split into two differents components. The intermediate pressure is set to the geometric mean of the high pressure and the low pressure as in Equation (10) thanks to a PI controller. Between the two compressors, the lean solution in mixed with the ammonia vapor in order to lower its temperature.

The same parameters than previously are applied to the simulation which runs with the cycle shown on Figure 17. The simulation converges toward the steady state after around 300 seconds.

Table 8 presents the results of the simulation.

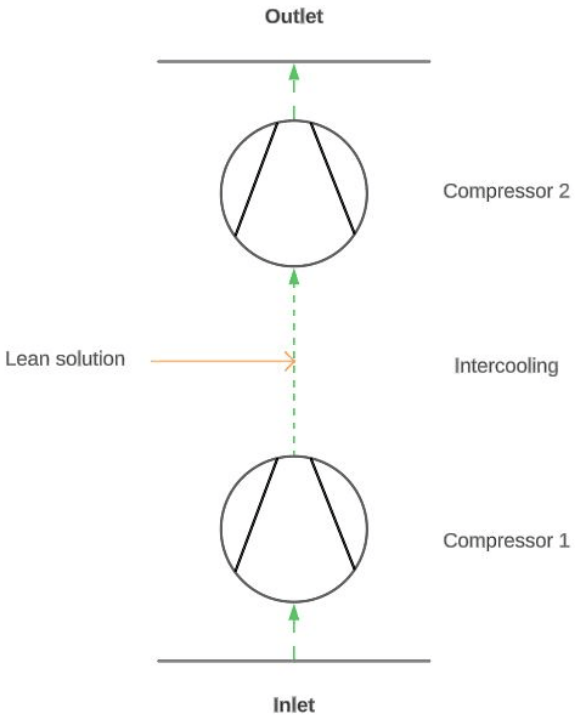

Figure 19: Injection of lean solution between the two compressor stages

Performance of the cycle

The characteristics of the cycle when the steady state is reached are as following :

- Rich solution water ratio : 0.35
- Lean solution water ratio : 0.61
- $Q_{Absorber,1}$: 59.3 kW
- $Q_{Absorber,2}$: 46.3 kW
- $Q_{sink} = Q_{Absorber,1} + Q_{Absorber,2}$: 105.6 kW
- $Q_{Desorber,1}$: 27.7 kW
- $Q_{Desorber,2}$: 46.0 kW
- $Q_{source} = Q_{Desorber,1} + Q_{Desorber,2}$: 73.7 kW
- Q_{IHX} : 3.2 kW

State point	Mass flow rate (kg/s)	Water mass fraction	Temperature (°C)	Pressure (bar)
1	0.138	0.35	57.8	5
2	0.061	0.02	57.8	5
2b	0.061	0.02	167	11.8
2i	0.070	0.09	99.9	11.8
3	0.070	0.09	**165**	26.9
4	0.077	0.61	57.8	5
5	0.077	0.61	58.8	26.9
5b	0.069	0.61	58.8	26.9
5i	**0.008**	0.61	58.8	26.9
6	0.069	0.61	68.8	26.9
7	0.138	0.35	125,2	26.9
8	0.138	0.35	74.5	26.9
9	0.138	0.35	69.9	26.9
10	0.138	0.35	27.1	5
11	0.5	1	65	1
12	0.5	1	29.7	1
13	0.5	1	65	1
14	0.5	1	115.2	1

Table 8: Simulation results of the cycle with the injection line

- Low pressure compressor speed : 50 Hz
- High pressure compressor speed : 100 Hz
- $W_{comp,low}$: 12.9 kW
- $W_{comp,high}$: 14.0 kW
- $W_{shaft,total}$: 26.9 kW
- W_{pump} : 0.51 kW

- Circulation ratio : 56 %
- Injection ratio (according to Equation (58)) : 13.5 %

$$r_{injection} = \frac{\dot{m}_{injected}}{\dot{m}_{comp,inlet}} \tag{58}$$

The COP can be derived from (34) :

$$COP = \frac{105.6}{26.9 + 0.51} = 3.85 \tag{59}$$

Effects of the injection ratio

In this model, the injection line is used to reduce the discharge temperature of the compressor. As explained in section 6, the maximum discharge temperature of the compressor indicated by the manufacturer is 180 °C in the facility. Figure (20) shows the discharge temperature with respect to the injection ratio. By varying the opening of the valve of the injection line, the injection ratio is changed on the range [0 - 0.4]. The discharge temperature gets lower than 180 °C from an injection ratio of 11.6 %. Then, from an injection ratio of around 18 %, the discharge temperature stabilizes at about 138 °C.

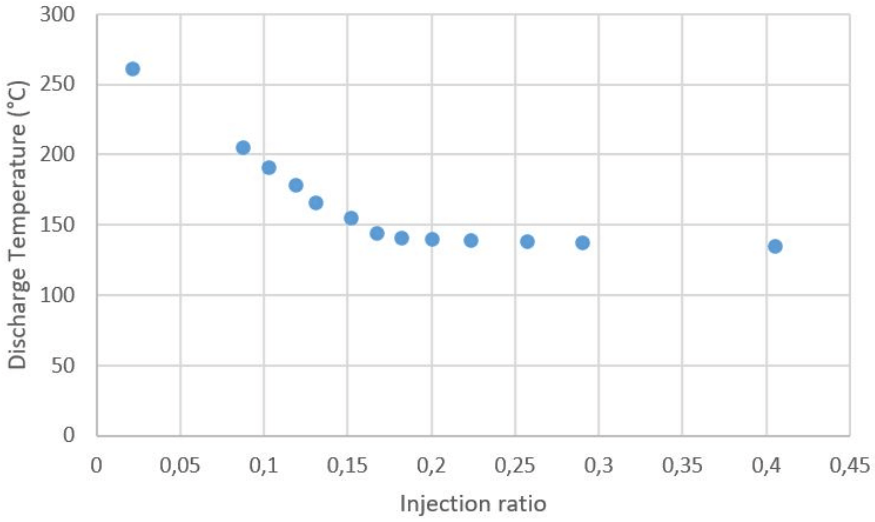

Figure 20: Discharge temperature of the compressor with respect to the injection ratio

Figure 21 shows the dependence between the COP and the injection ratio. When the injection ratio increases, the heat load decreases and the total shaft power of the compressor and the pump also decreases. As a result, the COP slightly increases with the injection ratio but this is not significant. An increase from 10 % to 30 % of the injection ratio leads to a growth of the COP of + 1 %.

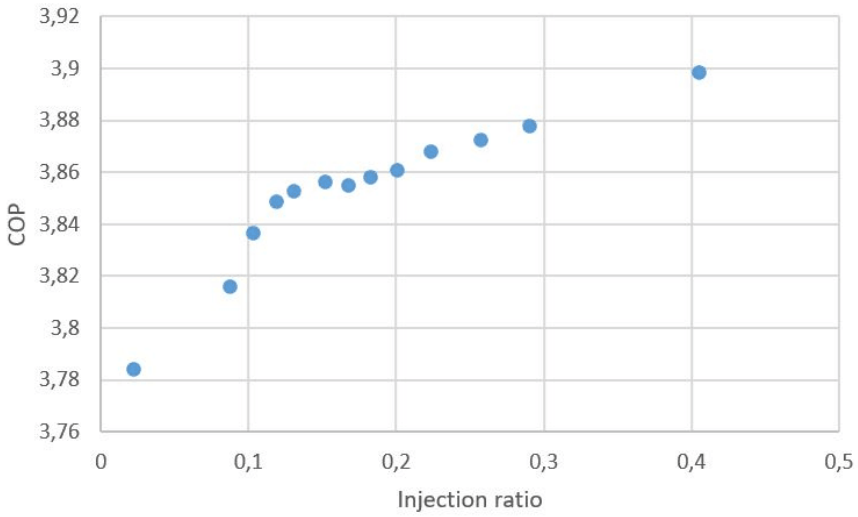

Figure 21: COP of the cycle with respect to the injection ratio

Effects of the sink outlet temperature

By varying the sink mass flow rate, is is possible to influence the sink outlet temperature and see its impact on the other parameters of the cycle. Figure 22 shows the dependence between the sink water mass flow rate and the sink outlet temperature. When the mass flow rate is 0.35 kg/s, the sink outlet temperature is 138 °C and when the mass flow rate is 0.8 kg/s, the outlet temperature goes down to 95.5 °C. The dependance between the mass flow rate and the outlet sink temperature is almost linear on this range of value. As expected, the outlet temperature decreases when the sink mass flow rate increases. On Figure 23, The COP is plot with respect to the temperature lift. For the simulations, the source inlet temperature remains constant at 65 °C and the temperature lift is defined as the temperature difference between the sink outlet temperature and the source inlet temperature. The COP decreases with the temperature lift varying from 4,47 at a temperature lift of 30 K to 3,2 at at a temperature lift of 73 K (-28 %). The shaft power of the compressor increases faster than the heat load when the temperature

lift goes up leading to a COP diminution. At the same time, the sink heat load increases when the temperature lift increases as shown on Figure 24. The heat load rises from 102.5 kW at a temperature lift of 30 K to 108.6 kW at 73 K (+ 6 %).

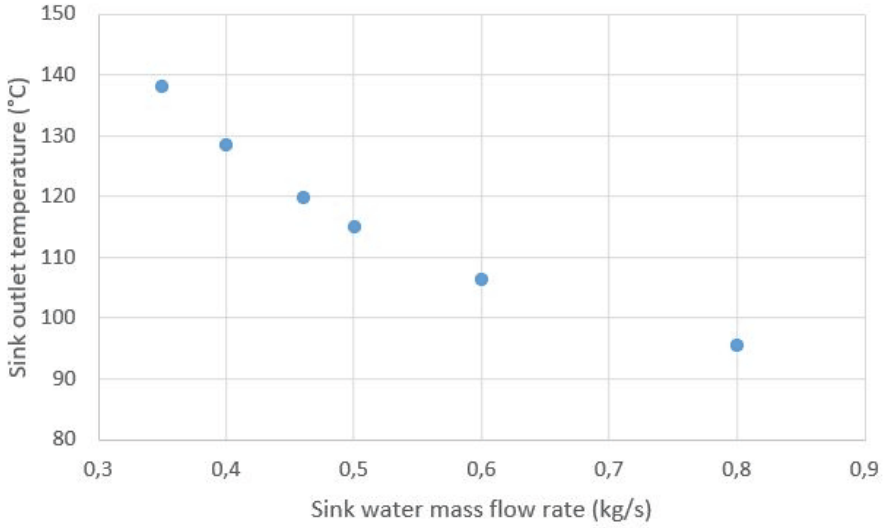

Figure 22: Outlet temperature of the sink with respect to its mass flow rate

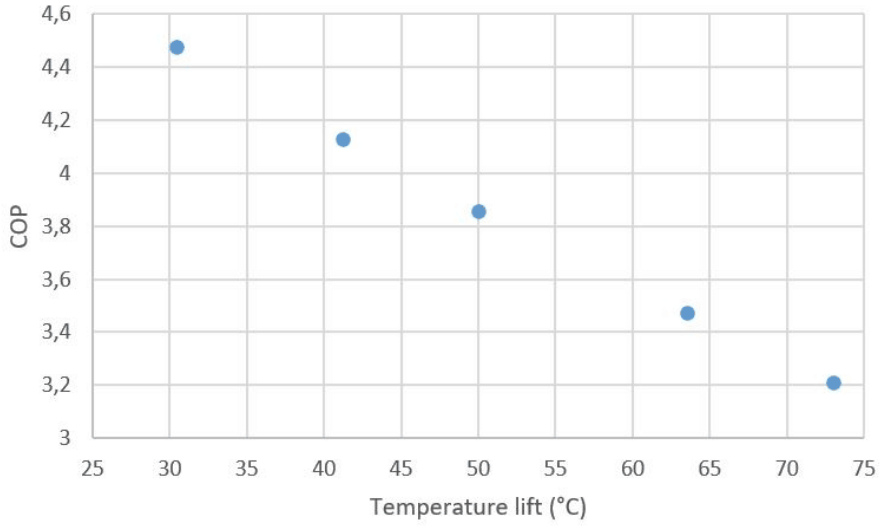

Figure 23: COP of the cycle with respect to the temperature lift

Figure 25 presents the discharge temperature and the discharge pressure with respect to the temperature lift. Both parameters increase with the temperature lift. The injection ratio was fixed at 13 % for all the simulations. When the sink outlet temperature gets higher, the inlet temperature of the absorber on the refrigerant side increases too and so are the discharge temperature and pressure.

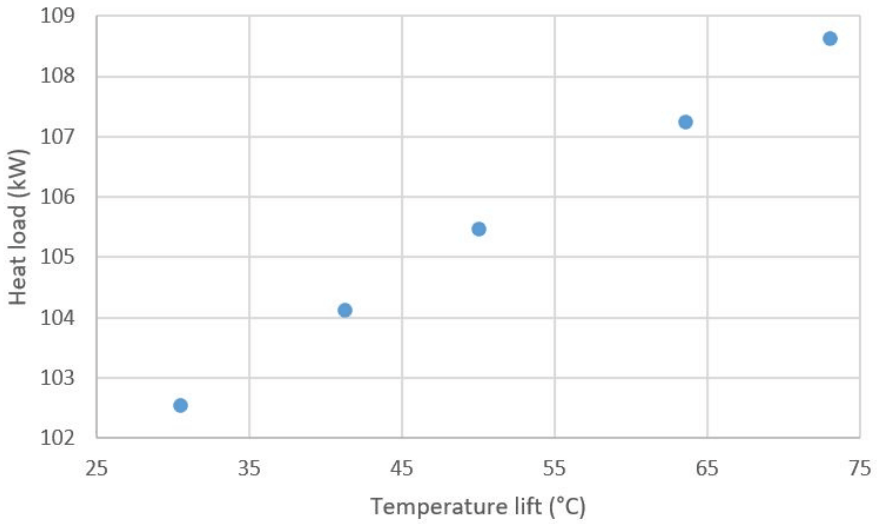

Figure 24: Heat load of the cycle with respect to the temperature lift

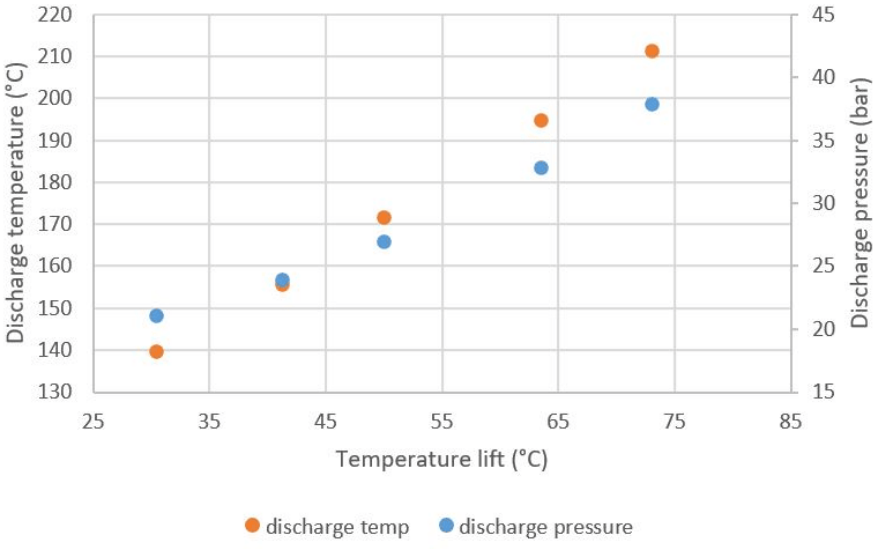

Figure 25: Discharge pressure and temperature with respect to the temperature lift

7.2.2 GHG analysis

The objective of this section is to evaluate the carbon emissions that could be avoided thanks to the simulated ACHP. Two scenarios will be considered : the first one with water being heated up from 65 °C to 95.5 °C and the second one with water being superheated from 65 °C to 120 °C. The amount of water considered in each case is 1 kg. In both scenarios, the equivalent carbon emission obtained with the heat pump will be compared to those obtained with an electric heater and a gas-fired boiler. Besides, a comparison will be conducted between the results obtained from an electricity mix of the USA, Europe and Norway. Table 9 presents the carbon equivalent emissions related to the electricity mix in the aforementioned location.

Producer	CO2 [g/kWh]	Source
Natural gas (World, 2022)	214	ADEME [29]
Electricity (US, 2022)	367	Ember-climate [30]
Electricity (Europe, 2022)	298	Ember-climate[30]
Electricity (Norway, 2022)	29	Ember-climate [30]

Table 9: Carbon intensity of the different hot water production modes

The following assumptions are made :

- Gas-fired boiler efficiency : 95 %
- Electric heater efficiency : 100 %

The energy necessary to heat up 1 kg of water is given by Equation (60).

$$E = (h_{sink,outlet} - h_{sink,inlet}) \tag{60}$$

Scenario 1 : sink outlet temperature of 95.5 °C

- Injection ratio : 12.5 %

- Temperature lift : 30 K
- Temperature sink inlet : 65 °C
- Temperature sink outlet : 95.5 °C
- COP : 4.47

E = 400.2 - 272.2 = 128 kJ

- $E_{gas,boiler}$: $\frac{128}{0.95} = 135\ kJ = 3.75.10^{-2}\ kWh$
- $E_{el,heater}$: $\frac{128}{1} = 128 = 3.55.10^{-2}\ kWh_{el}$
- $E_{ACHP} : E/COP = \frac{128}{4.47} = 28.6\ kJ_{el} = 7.77.10^{-3}\ kWh_{el}$

Scenario 2 : sink outlet temperature of 120 °C

This sink outlet temperature is the highest reached by the cycle for an injection ratio of 12.5 % and a dicharge temperature limited to 180 °C.

- Injection ratio : 12.5 %
- Temperature lift : 55 K
- Temperature sink inlet : 65 °C
- Temperature sink outlet : 120 °C
- COP : 3.71

In this scenario, the energy required to heat up 1 kg of water is : E = 2716.6-272.2 = 2444.4 kJ

- $E_{gas,boiler}$: $\frac{2444.4}{0.95} = 2573\ kJ = 0.71\ kWh$
- $E_{el,heater}$: $\frac{2444.1}{1} = 2444.4\ kJ_{el} = 0.68\ kWh_{el}$
- $E_{ACHP} : E/COP = \frac{2444.1}{3.71} = 659\ kJ_{el} = 0.18\ kWh_{el}$

The following table presents the summary of the carbon equivalent emissions for both scenario and for the electric mix associated to the different locations.

Scenario	Emissions in Scenario 1 (65°C - 95 °C) [gCO2eq]	Emissions in Scenario 2 (65°C - 120 °C) [gCO2eq]
Electricity boiler (US)	13	250
Electricity boiler (Europe)	11	203
Electricity boiler (Norway)	1	20
Gas-fired boiler (World)	8	152
ACHP (US)	2.8	66
ACHP (Europe)	2.3	54
ACHP (Norway)	0.2	5

Table 10: Summary of the carbon emissions equivalent associated to the heating of 1 kg of water in different scenarios and locations

7.3 Validation of the model

In order to validate the modeled Dymola cycle, the operating parameters of the experimental set of data has been set into the software. The objective is to evaluate the relevancy of the numerical model by comparing its performances to the actual values.

Thus, the simulation of the system was run according to the boundaries values presented in Table 5. The injection ratio was set to a reasonable value to make the simulation work.

Table 11 presents a comparison of the main features of the cycle. The comments on this table are in Section 8.

	Experimental cycle	Numerical cycle
Sink temperature glide	26.8 K	12 K
Sink temperature glide	8.5 K	8 k
Compressor discharge temperature	103.1 °C	98 °C
Pressure ratio	2.2	2.2 bar
Compressor shaft	11.8 kW	5.2
Pump power	0.7 kW	4.3
Heat load	29.4 kW	23.7 kW
COP	**2.35**	**2.49**

Table 11: Comparison of the main features of the experimental cycle and the Dymola model

8 Discussion

Experimental results

The analysis of the test made in the lab presented in section 7 presents numerous problems. Due to the breakage of the compressor before the end of the experiments in the facility, the data collected was not as relevant as expected. The steady-state was not reached in the experimental data collected and all the values were averaged which can lead to significant errors in the calculations. This leads to great errors in the calculations of the cycle features. For example, the heat transfered in the sink from the mixture is more than 1.7 times bigger than the heat load received by the water. The same problem takes place in the heat source. Besides, the ammonia-water ratio in the rich solution depends on the level in the high-pressure and in the liquid-vapor separator. As the enthalpy calculations depend on the ammonia-water ratio, if the levels are non-constant due to an unsteady state, the results might be inaccurate. Another problem is that the injection ratio during the test was way too high compared to its expected value. The mass flow rate injected was 0.075 kg/s compared to 0.024 kg/s at the inlet of the compressor. This represents an injection ratio of 300 % instead of a value that should be around 12.5 % according to both literature [10] and the results from the numerical modeling. The effect of this inappropriate injection ratio is that the volumetric efficiency is 13 % which is very low compared to values found in the literature that can go up to more than 95 % [24]. To get better results, a series of test should be run in the steady-state and the injection ratio should be set around 12.5 %.

Numerical modeling results

The objective of the numerical modeling was to implement a cycle that would behave like the NTNU facility to be able to compare and predict the functioning of the actual rig. The objective is also to find the optimal experimental parameters numerically. It is easier and cheaper to run numerical simulations than actual tests in the lab. At first, the most simple cycle was implemented with no internal heat

exchanger and no injection line. This basic cycle has a COP of 2.88 and a discharge temperature of the compressor of 250 °C. In order to increase the performance of the cycle, a second one was implemented with an internal heat exchanger. This second cycle has a COP of 3.79 which is 24 % higher than the previous one. This shows that the IHX allows to increase the performance significantly. The discharge temperature of the compressor is now of 284 °C. In order to model the lubrication and cooling of the compressor, a last cycle was implemented. This last cycle is the most complex and include an injection line. As it is not possible to model the direct injection of solution in the compressor with Dymola, this cycle includes a two-staged compressor and the lean solution from the pump is mixed with the vapor at the intermediate pressure. With this cycle, the coefficient of performance is increasing again to 3.85 (+1.5 %) compared to the one without the injection line. The most important feature is that the compressor discharge temperature is now down to reasonable values. Depending on the injection ratio, the discharge temperature can be lowered down under 180 °C which is the maximal temperature that the compressor can handle according to the manufacturer.

Comparison between the experimental cycle and the simulation

It can be observed in Table 11 that some of the parameters are very similar between the experimentation and the numerical modeling. The sink temperature glide, the pressure ratio and the heat load are alike in both cases. The mains differences stand in the sink temperature glide which is twice bigger for the experimental cycle and the compressor and pump required power. In the case of the facility, the compressor shaft power is 2.2 times bigger than in the simulation whereas the pump power required is more than 6 times bigger in the simulation than in the experiment. This is mainly because the quality at the outlet of the liquid-vapor separator is significantly higher in the simulation than in the experiment. Although the COP found for both cases are reasonably close to each other (+ 6 % in the numerical) The model seem reasonable even though there are some noticeable differences. The results would probably more similar if the experimental was run with better operating parameters and in a steady-state.

The differences between the numerical modeling and the experimental cycle

could also be related to errors from the simulation.

Sources of error in the simulation

As explained in section 6, the pressure drops in the heat exchangers have been neglected. The heat exchange between the pipes and the surrounding area has also been neglected in the whole cycle. These two reasons partly explain the higher COP found in the numerical model compared to the actual facility. Besides, the mixings have been assumed adiabatic which is also a hypothesis that improves the performance of the heat pump. Moreover, the high-pressure receiver has not been modeled in the simulation.

Greenhouse gas emissions

Thanks to Table 10, it is possible to evaluate the quantity of CO2 equivalent avoided with the ACHP on a certain period of time. To give an idea of the GHG emissions at stake, let us consider an industrial scale heat pump with a heat load of 1000 kW and the same performance than the ACHP under scrutiny. Considering a load factor of 40 % [31] throughout the year, the ACHP would be able to heat up 98.5 kT of water in Scenario 1 and and 5.2 kT in Scenario 2 per year. In scenario 1, this would results to up to 1260 TeqCO2 avoided compared to an electric boiler used in the US (if the ACHP run with the Norwegian electricity mix is used). In Scenario 2, the quantity of CO2 avoided can go up to 1274 TeqCO2 in the best case. This represents CO2 emissions reduced by up to 98.5 % in the first scenario and up to 98 % in the second scenario.

9 Conclusion

In conclusion, the food industry is a major contributor to greenhouse gas emissions and efforts to reduce these emissions must be a priority. Increasing energy efficiency and reducing the use of fossil fuels are key strategies for achieving climate neutrality in the food supply chain. High-temperature heat pumps, such as the ammonia-water absorption-compression heat pump, are a promising technology for both heat recovery and energy efficiency, and have the potential to be run with natural refrigerants such as ammonia that have a low global warming potential. The ACHP system has two main constraints concerning the efficiency and the heat sink temperature: the compressor and the heat exchangers. Simulations using Dymola showed that it was possible to reach COP up to 4.4 at a temperature lift of 30 K and up to 3.7 for a temperature lift of 55 K heating up water to 115 °C. The optimal injection ratio was found to be around 12 % when the lean solution is injected into the compressor. The set of data collected on the NTNU facility was not concluding because the compressor broke before proper results could be obtained. Although, promising results were achieved with the simulation and it can help predict the behavior of the actual cycle.

10 Further work

On the basis of the work conducted in this master thesis, the following propositions for further work are suggested :

Concerning the Dymola simulation :

- Perform the simulations with a cycle closer to the NTNU facility by using direct injection in the compressor. The next version of Dymola might have this component.
- Implement pressure drops in the heat exchangers to model more accurately the friction effects.
- Run the simulation with non-constant heat transfer coefficient in the heat exchangers.
- Implement a full control of the system on Dymola. More PI controller could be added in order to modify the variables automatically.

Besides, in parallel a work can be conducted on the experimental rig with the following objectives :

- Perform experiments with the HTHP cycle and try to reach the steady state.
- Run the cycle with the parameters found in the simulation and compare the performances.

11 Appendix

11.1 Facility

Figure 26 represents the process and instrumentation diagram of the facility.

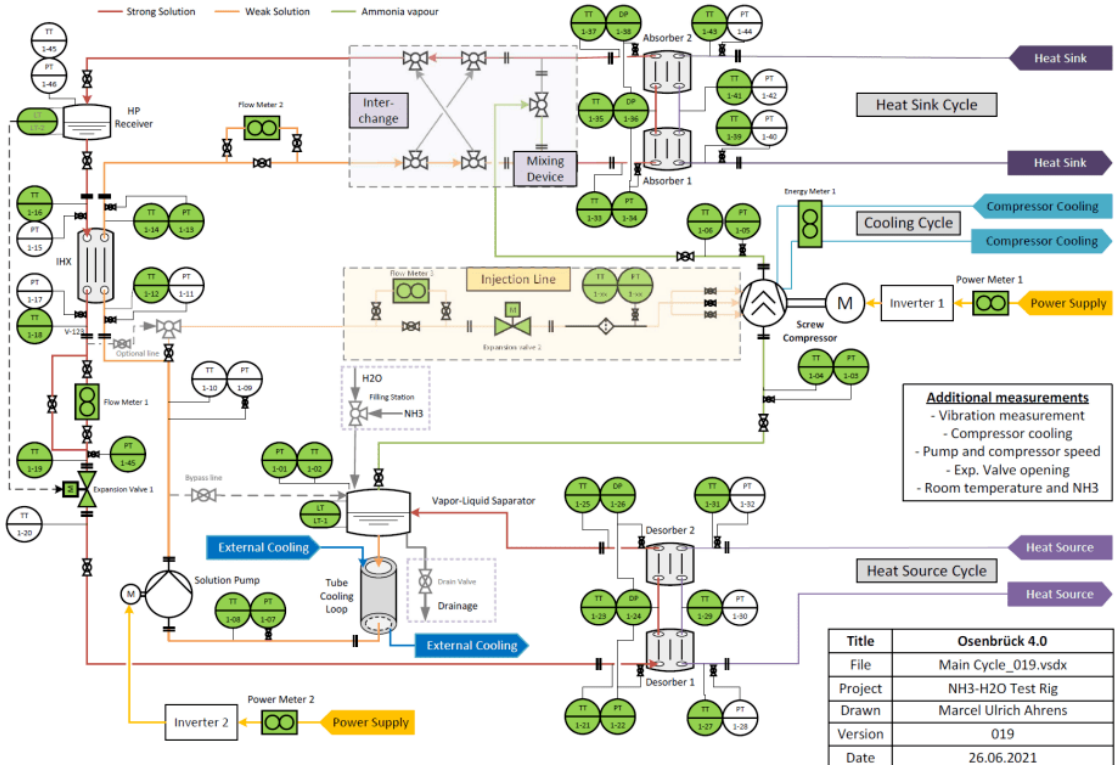

Figure 26: Process and instrumentation diagram of the main Osenbrück heat pump loop. From Ahrens [10]

.

11.2 Dymola simulations

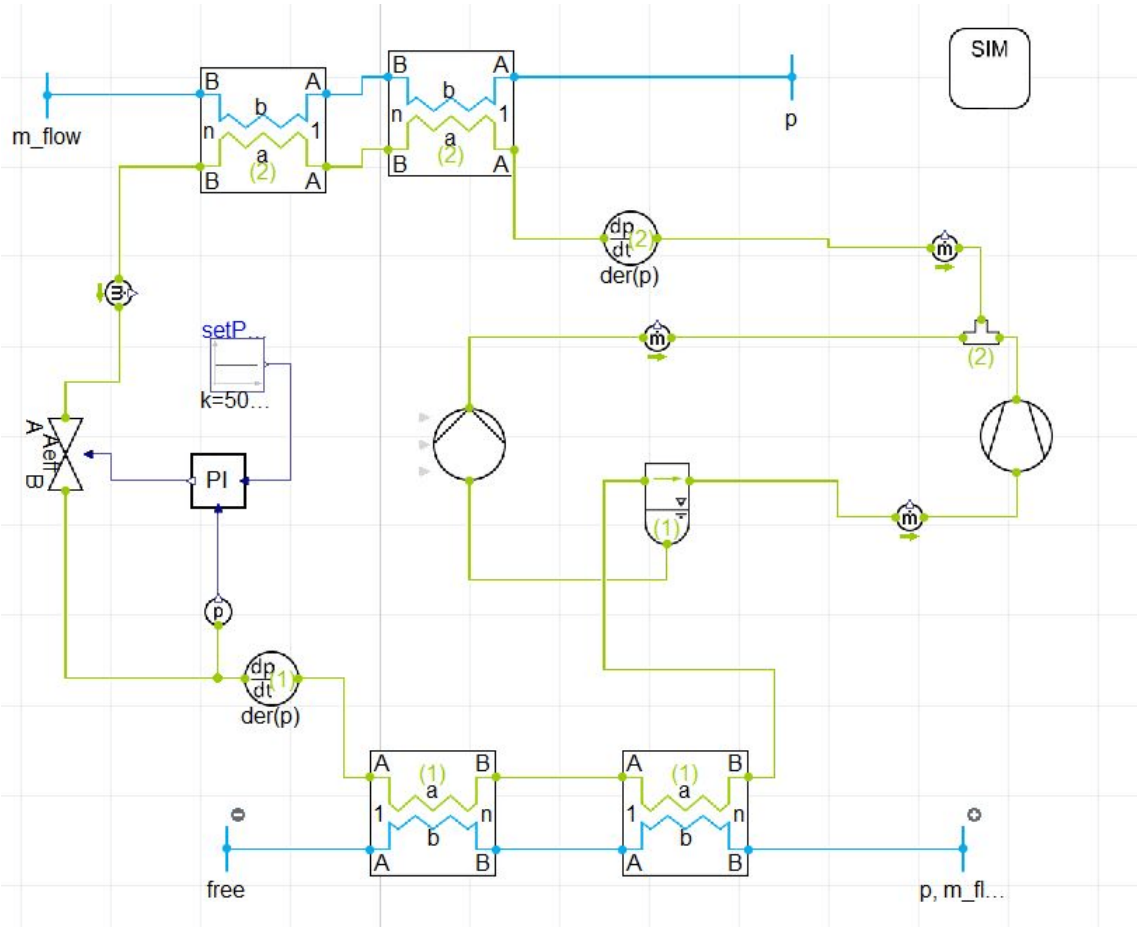

Figure 27: Dymola cycle without the IHX nor the injection line

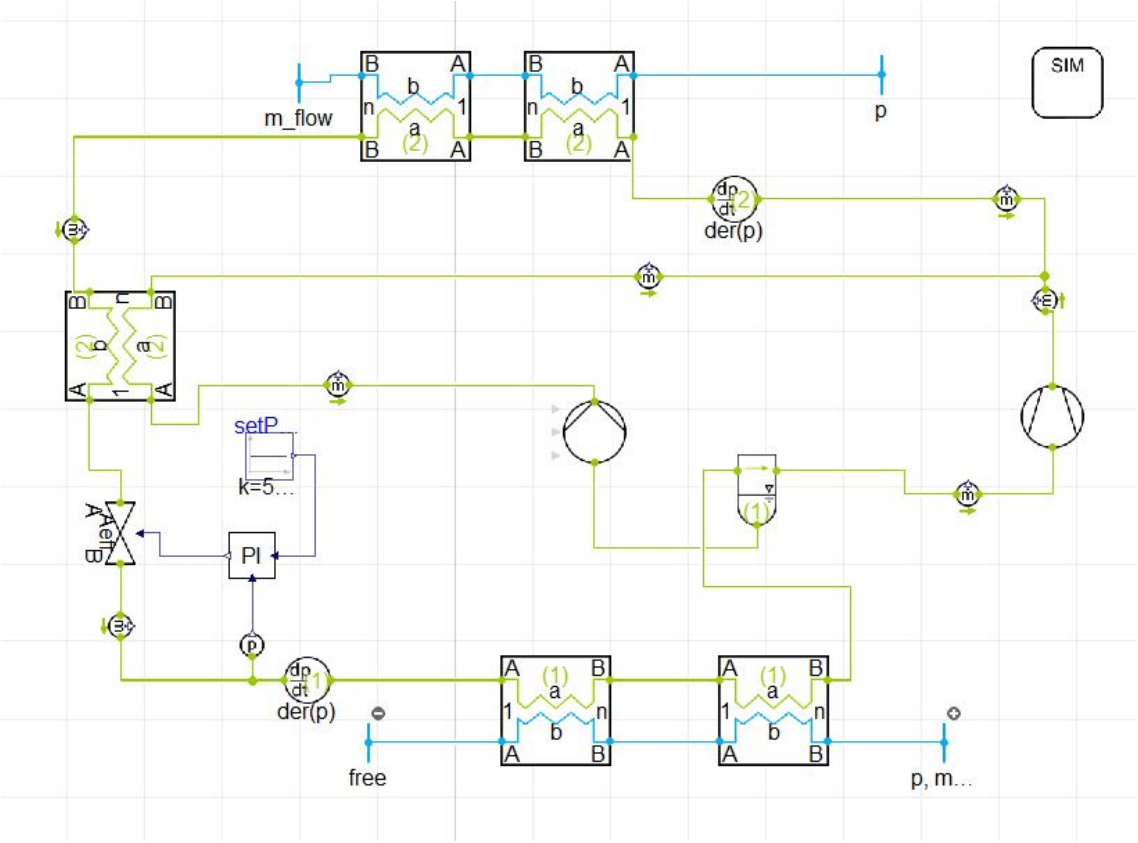

Figure 28: Dymola cycle with the IHX and without the injection line

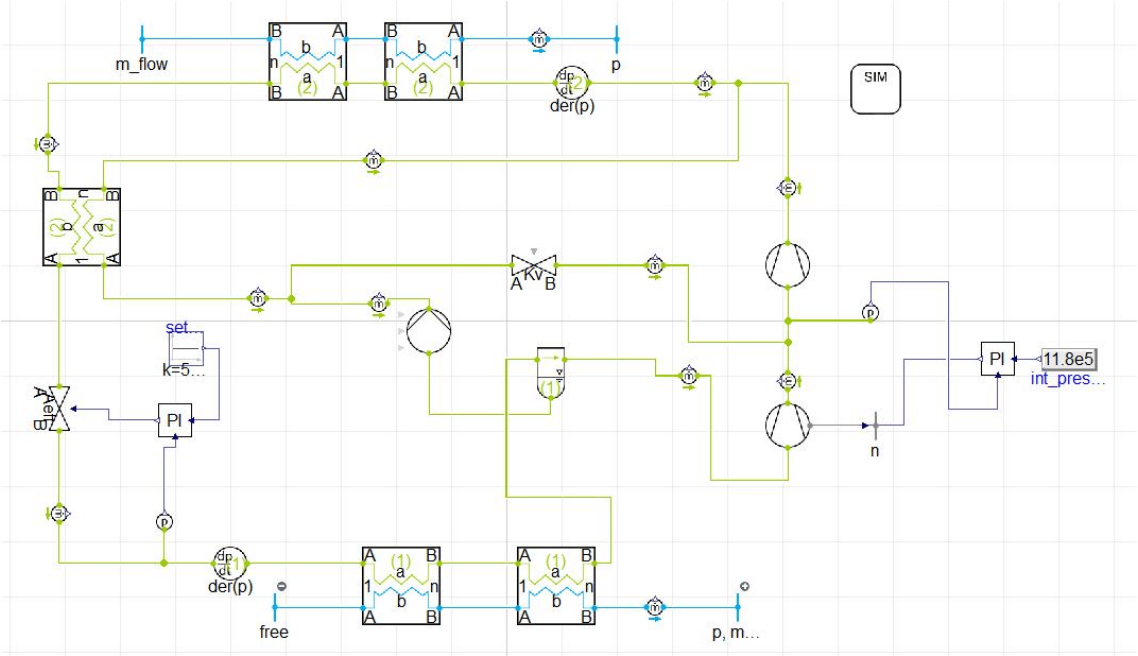

Figure 29: Dymola cycle with the injection line

11.3 Safety measures

General considerations about Ammonia

Anhydrous ammonia is a pungent, colourless gas at room temperature. The density of NH_3 at normal temperature and pressure is 0,77. The human physiological response to various concentrations of ammonia are listed in the following table

5 ppm	Least perceptible odour
20-50 ppm	Readily detectable odour
50-100 ppm	No discomfort or impairment of health for prolonged exposure
150-200 ppm	General discomfort and eye tearing ; no lasting effort on short exposure
400-700 ppm	Severe irritation of eyes, ears, nose, and throat
1700 ppm	Coughing, bronchial spasms
2000-3000 ppm	Dangerous, less than half an hour exposure may be fatal
5000-10 000 ppm	Serious edema, strangulation, asphyxia, rapidly fatal
10 000 ppm	Immediately fatal

Table 12: Physiological response of human body with respect to the ammonia concentration

At room temperature, the saturation pressure of ammonia is approximately 8 bar absolute. Therefore, the ammonia cylinders contain a saturated mixture of gas and liquid under a pressure of 8 bar. For piping and equipment, the material to avoid are copper, zinc and their alloys that can be corroded by ammonia in the presence of water vapor. Iron and steel are not affected by ammonia. The main risk from ammonia is exposure of operators to high concentrations exceeding 500 ppm that can occur because of sealing failure between high pressure cylinder and injector or because of a failure to follow the correct procedure while refilling the high pressure

side. Ammonia is flammable in a range of concentration between 16% and 25% by volume which is far above the toxicity limit. Therefore, no special considerations are to be taken concerning unintended combustion of NH_3.

The experimental area have numerous sources of dangers which require specific safety measures.

Flammable or reactive substances and gas

Flammable, reactive and pressurized substances or gases are in use in the facility. The maximum charge of ammonia water mixture in the rig is estimated to be under 50 kg. Initially, a vacuuming process takes place to evacuate the test rig. The risks of ammonia leakage are minimized thanks to a tight assembly of the system and appropriate ventilation. An ammonia concentration sensor connected to an alarm system is implemented as well as an ATEX-certified equipment for light. Stored as a pressurized liquid, ammonia can evaporate as a colorless gas at atmospheric pressure and a temperature of -32 °C. The following situations can lead to an incidental release or personal injury :

- Overfilling the tank
- Weakened undercarriage structure
- Faulty valves and deteriorated or out-of-date hoses
- External overheating of the storage container

In order to avoid personal injury, goggles, rubber gloves and other chemical resistant clothing are necessary when handling anhydrous ammonia.

Pressurized equipment

As there is pressurized equipment in use, the system must undergo pressure tests in accordance with the norms and be documented properly under the safety regulations. All components are pressure-tested for the given operating range. The maximum operating pressure in the rig is fixed at 16 bar for the low-pressure side and 40 bar for the high-pressure side.

Effects on the environment

An environmental impact is expected from the facility which can take the form of emissions, noise, temperature, vibration or smell. No emissions are expected during normal operation but NH_3 smell can be expected in case of leakage. NH_3 can be detected by humans above concentration of 25 ppm. The standard regulations indicate a risk of hazard level at concentrations above 500 ppm by volume on a 8-hour time-weighted average and a high hazard level above 5 000 ppm within the enclosure. Some recommendations are to be followed to avoid and handle ammonia leakages. A fixed ammonia alarm with a main alarm level below 500 ppm should be installed. Purging of NH_3 lines should be conducted before disconnection to avoid sudden releases of ammonia. This is achieved thanks to t sections on lines what will be purging.

There are two main potential sources of noise : the screw compressor and the motor. Equivalent products from other manufacturers indicate sound level up to 68 dB. Noise measurements can be performed during operation to determine the eventual need of corrective measures. Concerning hot temperatures, the maximum design temperatures is 180 °C. Hot pipes or components are insulated in order to prevent burns. A safety ventilation system is installed to regulate the amount of NH_3 in the air. The control and operation are done mainly from outside the room containing the rig. Noise protection shall be used when entering the room during operation.

First aid

Eyes or skin exposed to anydrous ammonia should be washed with water immediately and for at least 15 minutes. Contaminated clothing should be removed quickly and carefully. Water must be available in the area of the rig for flushing the eyes or skin in case of exposure.

Bibliography

[1] Marcel Ulrich Ahrens Maximilen Loth Ignat Tolstorebrov Armin Hafner Stefan Kabelac Ruzhu Wang and Trygve Magne Eikevik.
'Identification of Existing Challenges and Future Trends for the Utilization of Ammonia-Water Absorption-Compression Heat pump at High Tenperature Operation'. In: *Applied sciences* (2021).

[2] Timothée Dano. *Experimental investigation of ammonia-water heat pump*. 2022.

[3] Alia Serafim Bakalis Peter J. Fryer Estefania Lopez-Quiroga.
Mapping Energy Consumption in Food Manufacturing. 2019.

[4] J. Nordtvedt S.R. Horntvedt B. R. Eikefjord J. Johansen.
'HYBRID HEAT PUMP FOR WASTE HEAT RECOVERY IN NORWEGIAN FOOD INDUSTRY'.
In: *10th International Heat Pump Conference 2011* (2011).

[5] Marcel Ulrich AHRENS Hakon SELVNES Leon HENKE Michael BANTLE Armin HAFNER.
Investigation on heat recovery strategies from low temperature food processing plants : Energy analysis and system comparison. 2021.

[6] Marcel Ulrich Ahrens Sverre Stefanussen Foslie Ole Marius Moen Michael Bantle and Trygve Magne Eikevik.
'Integrated high temperature heat pumps and thermal storage tanks for combined heating and cooling in the industry'.
In: *Applied thermal engineering* (2021).

[7] Marcel Ulrich AHRENS Armin HAFNER and Trygve Magne EIKEVIK.
Development of Ammonia-Water Hybrid Absorption-Compression Heat Pumps. 2018.

[8] Marcel Ulrich AHRENS Armin HAFNER and Trygve Magne EIKEVIK.
Compressors for ammonia-water hybrid absorption-compression heat pumps. 2019.

[9] Stein Rune Nordvedt. *Experimental and theoretical study of a compression/absorption heat pump with ammonia/water as working fluid*. 2005.

[10] Marcel Ulrich. *Development of an ammonia-water absorption-compression heat pump at high temperature operation*. 2023.

[11] Michael Eckert Michael Kauffeld Volker Siegismund. *Natural refrigerants : Applications and practical guidelines*. 2019.

[12] J.K. Reinholdt L. Markussen W.B. Elmegaard B. Jensen. 'Investigation of ammonia/water hybrid absorption/compression heat pumps for heat supply temperatures above 100 °C'. In: *ISHPC 2014* (2014).

[13] Jensen Jonas Kjaer. *Industrial heat pumps for high temperature process applications*. 2016.

[14] Jensen Jonas K. Ommen Torben Reinholdt Lars Markussen Wiebke B. Elmegaard Brian. 'Heat pump COP, part 2: Generalized COP estimation of heat pump processes'. In: *Proceedings of the13th IIR-Gustav Lorentzen Conference on Natural Refrigerants* (2018).

[15] Hongzhi Yan Ruzhu Wang Shuai Du Bin Hu and Zhenyuan Xu. 'Analysis and perspective on Heat Pump for industrial Steam generation'. In: *Advanced Energy and Sustainability Research* (2021).

[16] C. H. M. Machielsen L. C. M. Itard. *Considerations when modelling compression/resorption heat pumps*. 1994.

[17] Reinhard Radermacher Milind V. Rane Karim Amrane. *Performance enhancement of a two-stage vapour compression heat pump with solution circuits by eliminating the rectifier*. 1992.

[18] R. Radermacher E.A. Groll. *Vapor Compression heat pump with solution circuit and desorber/absorber heat exchange*. 1994.

[19] Marcel Ulrich AHRENS Ivar S. ERTESVAG and Trygve Magne EIKEVIK. *Exergy analysis of combined absoption-compression heat pump with ammonia-water mixture as a working fluid*. 2020.

[20] Yong Tae Kang Atsushi Akisawa Takao Kashiwagi. *Analytical investigation of two different absorption modes: falling film and bubble types*. 2000.

[21] B. Markmann T. Tokan M. Loth J. Stegmann K.H. Hartmann H. Kruse S. Kabelac.
Experimental results of an absorption-compression heat pump using the working fluid ammonia-water for heat recovery in industrial processes. 2019.

[22] K. Amrane M. V. Rane R. Radermacher. *Performance Curves for Single-Stage Vapor Compression Cycles With Solution Circuit*. 1991.

[23] J. Stene. *Design and application of ammonia heat pump systems for heating and cooling of non-residential buildings*. 2008.

[24] Trygve Magne Eikevik Marcel Ulrich Ahrens Ignat Tolstorebrov Even Kristian Tønsberg Armin Hafner R.Z. Wang.
Numerical investigation of an oil-free liquid-injected screw compressor with ammonia-water as refrigerant for high temperature heat pump applications. 2023.

[25] H Martin. 'A theoretical approach to predict the performance of chevron-type plate heat exchangers'.
In: *Chemical Engineering and Processing: Process Intensification* (1996).

[26] F. Táboas M. Vallès M. Bourouis A. Coronas. 'Flow boiling heat transfer of ammonia/water mixture in a plate heat exchanger'.
In: *International Journal of Refrigeration* (2010).

[27] L. Silver. 'Gas cooling with aqueous condensation: A new procedure for calculating heat transfer coefficients'. In: *The Industial Chemist* (1947).

[28] K. J. Bell M. A. Ghaly. 'An approximate generalized design method for multicomponent/partial condensers'.
In: *13th National Heat Transfer Conference,* (1972).

[29] *Base empreinte, Agence de l'Environnement et de la Maîtrise de l'Energie Facteur d'émission / Indicateur GES*. https://base-empreinte.ademe.fr/. Accessed: 2023-06-04.

[30] *Ember climate Data catalogue*. https://ember-climate.org/.
Accessed: 2023-06-04.

[31] Helge Averfalk Paul Ingvarsson Urban Persson Mei Gong Sven Werne.
'Large heat pumps in Swedish district heating systems'. In: (2017).

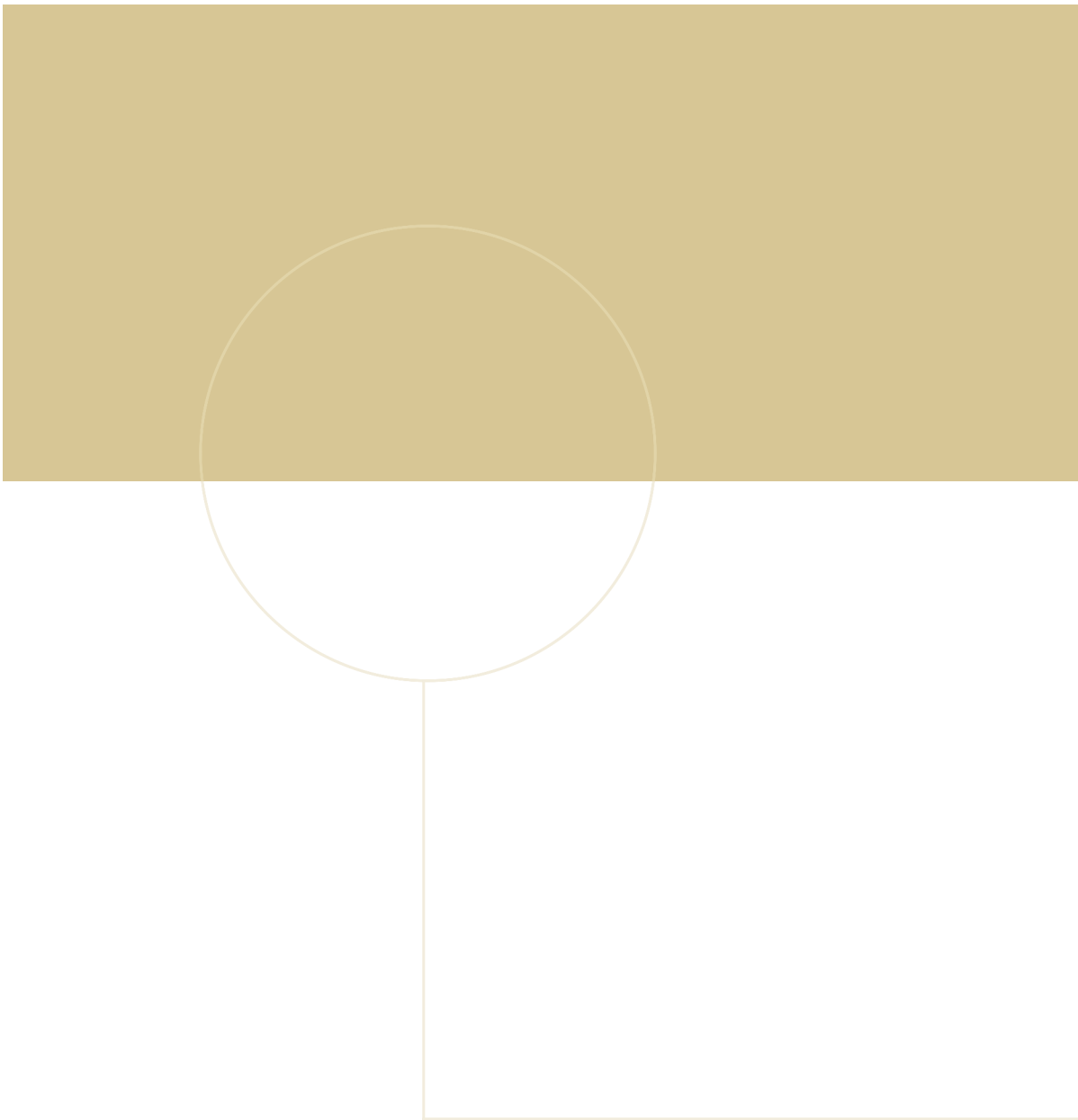

NTNU

Norwegian University of
Science and Technology